

Stationarity preserving nodal Finite Element methods for multi-dimensional linear hyperbolic balance laws via a Global Flux quadrature formulation

Wasilij Barsukow^a, Mario Ricchiuto^b, Davide Torlo^c

^aInstitut de Mathématiques de Bordeaux (IMB), CNRS UMR 5251,
351 Cours de la Libération, 33405 Talence, France - wasilij.barsukow@math.u-bordeaux.fr

^bINRIA, Univ. Bordeaux, CNRS, Bordeaux INP, IMB, UMR 5251,
200 Avenue de la Vieille Tour, 33405 Talence cedex, France - mario.ricchiuto@inria.fr

^cDipartimento di Matematica G. Castelnuovo,
Università di Roma La Sapienza, Roma, Italy - davide.torlo@uniroma1.it

October 6, 2025

Abstract

We consider linear, hyperbolic systems of balance laws in several space dimensions. They possess non-trivial steady states, which result from the equilibrium between derivatives of the unknowns in different directions, and the sources. Standard numerical methods fail to account for this equilibrium, and include stabilization that destroys it. This manifests itself in a diffusion of states that are supposed to remain stationary. We derive new stabilized high-order Finite Element methods based on a Global Flux quadrature: we reformulate the entire spatial operator as a mixed derivative of a single quantity, referred to as global flux. All spatial derivatives and the sources are thus treated simultaneously, and our methods are stationarity preserving. Additionally, when this formulation is combined with interpolation on Gauss-Lobatto nodes, the new methods are super-convergent at steady state. Formal consistency estimates, and strategies to construct well-prepared initial data are provided. The numerical results confirm the theoretical predictions, and show the tremendous benefits of the new formulation.

1 Introduction

This paper focuses on the discretization of multi-dimensional hyperbolic balance laws. Our final aim is to be able to treat non-linear PDEs such as the Euler equations with gravity, friction or chemical reactions, or the shallow water equations with bathymetric, Coriolis, and wind stress source terms. Having in mind this objective, in this work we consider the simpler setting of linear hyperbolic balance laws, and in particular the linear wave equation in first-order form with general source terms:

$$\begin{cases} \partial_t \mathbf{v} + \nabla p = \mathbf{S}_v, & \mathbf{v}: \Omega \subset \mathbb{R}^d \rightarrow \mathbb{R}^d, \\ \partial_t p + \nabla \cdot \mathbf{v} = S_p, & p: \Omega \subset \mathbb{R}^d \rightarrow \mathbb{R}. \end{cases} \quad (1)$$

In $d = 2$ space dimensions, we write

$$\begin{cases} \partial_t u + \partial_x p = S_u, \\ \partial_t v + \partial_y p = S_v, \\ \partial_t p + \partial_x u + \partial_y v = S_p, \end{cases} \quad (2)$$

for $u, v, p: \Omega \subset \mathbb{R}^2 \rightarrow \mathbb{R}$, and with $\mathbf{v} = (u, v)$ and $\mathbf{S}_{\mathbf{v}} = (S_u, S_v)$. These equations can be used as toy-models for more complex systems such as the shallow water equations, Euler equations, and magneto-hydrodynamics.

We also introduce the compact form

$$\partial_t \mathbf{Q} + \nabla \cdot \mathbf{F} = \mathbf{S}, \quad \mathbf{F} = (J^x \mathbf{Q}, J^y \mathbf{Q}) \quad (3)$$

of the system (1) with, in two space dimensions,

$$\mathbf{Q} = \begin{pmatrix} u \\ v \\ p \end{pmatrix}, \quad J^x = \begin{pmatrix} 0 & 0 & 1 \\ 0 & 0 & 0 \\ 1 & 0 & 0 \end{pmatrix}, \quad J^y = \begin{pmatrix} 0 & 0 & 0 \\ 0 & 0 & 1 \\ 0 & 1 & 0 \end{pmatrix}, \quad \mathbf{S} = \begin{pmatrix} S_u \\ S_v \\ S_p \end{pmatrix}. \quad (4)$$

System (1) admits non-trivial stationary states governed by the conditions

$$\nabla \cdot \mathbf{v} = S_p, \quad (5)$$

$$\nabla p = \mathbf{S}_{\mathbf{v}}. \quad (6)$$

1.1 Well balanced and stationarity preserving methods in multiple dimensions

An important challenge in numerics for hyperbolic PDEs is to find a stabilization for numerical methods such that the solution is not entirely dissipated in long-time simulations. Typical applications of such PDEs require studying the long-time evolution of perturbations of stationary states, without any spurious numerical waves. To address this challenge, we aim at numerical methods capable of providing enhanced approximations of genuinely multi-dimensional stationary states.

This is already a complicated task when considering the homogeneous version of (2). As we will explain shortly, with classical stabilization strategies data needs to fulfill $\partial_x u = 0$ and $\partial_y v = 0$ to remain stationary, i.e. classical methods keep stationary only an insignificant subset of all divergence-free vector fields $\partial_x u + \partial_y v = 0$. Numerical methods whose stationary states are described by a discretization of $\nabla \cdot \mathbf{v} = 0$ without further constraints possess a rich set of stationary states and are called stationarity preserving [8]. One can show that the low Mach number limit of the Euler equations is related to the long-time limit of linear acoustics [32, 33], and that stationarity preserving methods are also involution preserving [8].

Classical stabilization operators are inspired by the smoothing associated to parabolic regularization. To first order, for the homogeneous vector equation in (1), in the simplest setting the stabilization is of the form

$$\partial_t u + \partial_x p = \frac{h}{2} \partial_x^2 u, \quad (7)$$

$$\partial_t v + \partial_y p = \frac{h}{2} \partial_y^2 v, \quad (8)$$

having denoted by h the mesh size. One can immediately verify that, unless $\partial_x u = \partial_y v = 0$, divergence-free vector fields are not preserved as $\nabla \cdot \mathbf{v} = 0$ is not a stationary solution of the stabilized problem. The difficulties essentially come about because one-dimensional stabilization is used in a multi-dimensional context. A way to re-establish consistency is to account for the multidimensional coupling of the velocity components, and replace the above stabilization by a gradient of the divergence. This leads to a vector Laplacian stabilization of the form [45, 50, 31, 44, 37, 8, 10]

$$\partial_t \mathbf{v} + \nabla p = \frac{h}{2} \nabla (\nabla \cdot \mathbf{v}) = \frac{h}{2} \begin{pmatrix} \partial_x^2 u + \partial_x \partial_y v \\ \partial_x \partial_y u + \partial_y^2 v \end{pmatrix}.$$

Observe that this way, mixed derivatives ∂_{xy} appear, i.e., this is a truly multi-dimensional stabilization, and it reduces to the previous stabilization in purely one-dimensional situations. While modified equation analysis gives a hint of what needs to be done in the fully discrete setting, it is not sufficient. Instead, as

shown in [10], one needs to ensure that the same discrete divergence is in the kernel of both the unstabilized discrete divergence operator, and of the discrete stabilization. In [8] a general way of achieving this in the context of Finite Difference methods was presented, and in [10] this was achieved for the streamline upwind Petrov-Galerkin (SUPG) method.

For balance laws, the stabilization needs to take into account the source terms, since it is no longer the solenoidal constraint that needs to be satisfied, but (5). The corresponding generalization of conformal approaches focused on the solenoidal condition is far from trivial. This is why most effective multi-dimensional stationarity preserving schemes for systems of balance laws to this date rely on correction techniques that require the precise knowledge of the steady solution [25, 11, 28, 13, 23].

1.2 Multidimensional Global Flux quadrature

In this work, we extend [10], which is dedicated to preserving divergence-free equilibria, to linear problems with source terms. Our approach exploits the Global Flux (GF) idea [27, 14, 16, 17, 18], originally tailored for one-dimensional balance laws, and developed for Finite Volume [27, 16, 17, 18], Discontinuous Galerkin [38], Finite Differences [34], and stabilized Finite Element methods [39]. Relations with other approaches, such as e.g. Residual Distribution schemes, are discussed in [4].

For one-dimensional hyperbolic balance laws of the form

$$\partial_t Q + \partial_x F(Q) = S(x, Q) \quad (9)$$

the GF approach amounts to discretizing, instead of (9), the equivalent problem

$$\partial_t Q + \partial_x G(x, Q) = 0, \quad \text{with } G(x, Q) := F(Q) - \underbrace{\int_{x_0}^x S(s, Q(s, t)) ds}_{=: K(x, Q)}. \quad (10)$$

At the discrete level, it means that there is only one differential operator discretizing ∂_x , while discrete equilibria are fully determined by the approximation of the source integral K . As shown in [4], the simplest of such methods is the usual source term upwinding which dates back to the early ideas of Roe [49], and early works on the so-called C-property [12]. In certain cases, they can be explicitly and fully described, independently on the discretization of ∂_x , using ODE integration methods [38, 34].

The above framework is purely one dimensional. The first genuinely multi-dimensional and arbitrarily high-order generalization is discussed in [10] in the context of nodal, continuous, stabilized Finite Element methods. A (low order) Finite Volume version of the same is proposed in [9]. The present work incorporates source terms in the multi-dimensional setting and aims at designing arbitrarily high-order Finite Element formulations that preserve the corresponding multi-dimensional discrete equilibria. To this end, the main idea is to rewrite the last equation of (2) as

$$\partial_t p + \partial_{xy} \left(\int_{y_0}^y u(x, s) ds \right) + \partial_{xy} \left(\int_{x_0}^x v(s, y) ds \right) - \partial_{xy} \left(\int_{x_0}^x \int_{y_0}^y S_p(s_1, s_2) ds_2 ds_1 \right) = 0.$$

Setting

$$\begin{cases} \mathcal{U}(x, y) := \int_{y_0}^y u(x, s) ds, \\ \mathcal{V}(x, y) := \int_{x_0}^x v(s, y) ds, \\ \mathcal{K}_p(x, y) := \int_{x_0}^x \int_{y_0}^y S_p(s_1, s_2) ds_2 ds_1 \end{cases} \quad (11)$$

and

$$G_p := \mathcal{U} + \mathcal{V} - \mathcal{K}_p, \quad (12)$$

we obtain

$$\partial_t p + \partial_{xy} G_p = 0. \quad (13)$$

(12) is a genuinely multi-dimensional GF accounting also for source terms. As we will show below, although equivalent to (2), formulation (13) is significantly more effective for obtaining stationarity preserving methods.

The pressure gradient balance (6) is treated here using one-dimensional global integration independently on the x and y directions, i.e.,

$$\mathcal{K}_{\mathbf{v}} = (\mathcal{K}_u, \mathcal{K}_v) = \left(\int_{x_0}^x S_u(s, y) ds, \int_{y_0}^y S_v(x, s) ds \right). \quad (14)$$

Altogether, one obtains the following multi-dimensional GF model

$$\begin{cases} \partial_t u + \partial_x(p - \mathcal{K}_u) = 0, \\ \partial_t v + \partial_y(p - \mathcal{K}_v) = 0, \\ \partial_t p + \partial_{xy} G_p = 0, \end{cases} \quad (15)$$

which is equivalent to (2), and which will serve as the basis of discretization as shown below.

Stationary states of (15) are characterized by

$$\begin{aligned} G_p &= \sigma_p^x(x) + \sigma_p^y(y), \\ p - \mathcal{K}_u &= \sigma_u^y(y), \\ p - \mathcal{K}_v &= \sigma_v^x(x), \end{aligned} \quad (16)$$

for arbitrary functions $\sigma_p^x, \sigma_p^y, \sigma_u^y, \sigma_v^x: \mathbb{R} \rightarrow \mathbb{R}$ that depend on the boundary conditions. The truly multi-dimensional condition $\nabla \cdot \mathbf{v} = S_p$ is now replaced by imposing that $G_p = \mathcal{U} + \mathcal{V} - \mathcal{K}_p$ is a sum of a function in x and a function in y , and similarly, (6) is replaced by imposing that $p - \mathcal{K}_u$ and $p - \mathcal{K}_v$ vary only in y and x , respectively. One could say that we have rewritten the model in such a way that dimensional splitting is no longer a problem. Of course, in the end, a dimensionally split method for the GF formulation (15) will yield a truly multi-dimensional method for the original formulation (2).

Finally, we would like to remark that firstly, the above reformulation is used to modify the quadrature appearing in the discretization. This is why this method is better referred to as a Global Flux quadrature approach. Moreover, the wording global refers to the coupling between all the different terms in the PDE, and must not be confused with the presence of global, integrated quantities. Indeed, at discrete level only differences of them will appear, the lower integration bound can be chosen differently in each cell, and the resulting method is local, with a usual size of the stencil.

1.3 Main contribution and outline of the paper

In this paper, we propose to start from (15) to construct, analyze, and implement new numerical methods with enhanced stationarity preserving properties for multi-dimensional hyperbolic balance laws. In Section 2, we discuss the types of source terms that we will include, and give some insights into the properties of the exact steady states, with a focus on the boundary conditions. Section 3 introduces the discrete framework of continuous tensor nodal Finite Elements, the standard Galerkin variational forms, and stabilization based on the SU and OSS methods. In Section 4, we introduce the novel multi-dimensional GF framework into the Galerkin discrete variational statement. We prove the structure preserving properties of the new discrete equations, and give a strong characterization of the discrete equilibria, including an explicit definition and estimates of their nodal consistency properties, and we analyze the interplay between them and the boundary conditions. We then discuss how to modify the stabilization terms such that they are compatible with the discrete equilibria in Section 5. This extends the work of [10] by accounting for forcing terms of different forms (in particular, not only Coriolis-type). In Section 6, we introduce the Deferred Correction time discretization that allows to obtain arbitrarily high-order schemes while maintaining the equilibria as steady states. Section 7 shows numerical benchmarks up to order 6 confirming the dramatic enhancements brought by our approach. Section 8 ends with open issues and future research directions.

2 Examples of steady states

In this section we review the types of steady equilibria we wish to approximate numerically. Besides the satisfaction of the partial differential equation, these solutions may require the specification of appropriate boundary conditions when they do not have a compact support.

System (2) involves both a vector source term \mathbf{S}_v , and a scalar source term S_p . The latter is essentially a pressure/mass pulsation, while the vectorial source can be seen as a force/acceleration. The former will be assumed to be of the following general form:

$$\mathbf{S}_v = c(x, y)\mathbf{v}^\perp - f(x, y)\mathbf{v} + \boldsymbol{\tau}(x, y) \quad (17)$$

with $c, f : \mathbb{R}^2 \rightarrow \mathbb{R}^+$, $\boldsymbol{\tau} : \mathbb{R}^2 \rightarrow \mathbb{R}^2$, having set $\mathbf{v}^\perp = (v, -u)$. The first term models a Coriolis force, the second friction, the last external forcing.

The stationary states are then governed by

$$\nabla p = \mathbf{S}_v = c(x, y)\mathbf{v}^\perp - f(x, y)\mathbf{v} + \boldsymbol{\tau}(x, y), \quad (18)$$

$$\nabla \cdot \mathbf{v} = S_p, \quad (19)$$

from which it follows that the curl of \mathbf{S}_v has to vanish at steady state:

$$0 = \nabla^\perp \cdot \mathbf{S}_v = c(x, y)S_p - f(x, y)\nabla^\perp \cdot \mathbf{v} + \nabla^\perp \cdot \boldsymbol{\tau}(x, y) + \mathbf{v} \cdot (\nabla c(x, y) - \nabla^\perp f(x, y)), \quad (20)$$

with $\nabla^\perp := (\partial_y, -\partial_x)$; observe that $\nabla^\perp \cdot \mathbf{v}^\perp = \nabla \cdot \mathbf{v}$.

Another relation at steady state is obtained by combining the steady states of the first two equations in (2), and integrating them in x and y :

$$p(x, y) = \int_{x_0}^x S_u dx + p(x_0, y) = \int_{y_0}^y S_v dy + p(x, y_0), \quad (21)$$

where $p(x, y)$ denotes the pressure at equilibrium. This can be recast as

$$p(x, y) - \{\lambda p(x_0, y) + (1 - \lambda)p(x, y_0)\} = \lambda \int_{x_0}^x S_u dx + (1 - \lambda) \int_{y_0}^y S_v dy, \quad \forall \lambda \in \mathbb{R}. \quad (22)$$

The above relations highlight a coupling between the different variables via the boundary conditions. More generally, using the structure of the equations, and the general form of the steady solutions, one can derive compatibility relations between boundary pressure, and boundary velocities. This allows to set conditions on either of the variables independently on what data is given on the boundaries. In the following, we study in more detail three types of moving equilibria that can be obtained with different source terms. Compatibility relations for the pressure/velocity boundary values at steady state are provided for each of them.

2.1 Steady states with Coriolis term only

This is a classical case studied also in recent works using other approaches [6, 5, 14]. Introducing only the Coriolis source term (i.e. $f = 0$, $\tau = 0$, $S_p = 0$), the equilibria can be described by

$$\begin{cases} \partial_x p - cv = 0, \\ \partial_y p + cu = 0, \\ \partial_x u + \partial_y v = 0. \end{cases} \quad (23)$$

These include an interaction between the pressure and the velocities. In particular, if the boundary conditions are prescribed on the pressure $p(x, y_0)$ and $p(x_0, y)$, then we can see from (21) that

$$\begin{cases} p(x, y) - \int_{x_0}^x c(s, y)v(s, y)ds = p(x_0, y), \\ p(x, y) + \int_{y_0}^y c(x, s)u(x, s)ds = p(x, y_0), \\ \mathcal{U} + \mathcal{V} = \sigma_p^x(x) + \sigma_p^y(y). \end{cases} \quad (24)$$

where σ_p^x and σ_p^y are arbitrary functions of x and y , respectively. The first two equations imply

$$\int_{x_0}^x c(s, y) v(s, y) ds + \int_{y_0}^y c(x, s) u(x, s) ds = p(x, y_0) - p(x_0, y). \quad (25)$$

If the Coriolis coefficient c is constant, then (25) implies

$$\mathcal{U} + \mathcal{V} = \frac{p(x, y_0) - p(x_0, y)}{c} \Rightarrow \sigma_p^x(x) = \frac{p(x, y_0)}{c}, \quad \sigma_p^y(y) = -\frac{p(x_0, y)}{c}. \quad (26)$$

In case the boundary conditions are given on the velocities, we now have

$$\begin{cases} p(x, y) - \int_{x_0}^x c(s, y) v(s, y) ds = \sigma_u^y(y) = p(x_0, y), \\ p(x, y) + \int_{y_0}^y c(x, s) u(x, s) ds = \sigma_v^x(x) = p(x, y_0), \end{cases} \quad (27)$$

where $\sigma_v^x(x) = p(x, y_0)$ and $\sigma_u^y(y) = p(x_0, y)$ are to be determined. To combine the two relations we evaluate the first for $y = y_0$, and the second for $x = x_0$. Setting $p_0 = p(x_0, y_0)$ we can write the compatibility relations:

$$\sigma_u^y(y) = p(x_0, y) = p_0 - c \int_{y_0}^y u(x_0, s) ds, \quad \sigma_v^x(x) = p(x, y_0) = p_0 + c \int_{x_0}^x v(s, y_0) ds. \quad (28)$$

For constant c , inspired by the tests proposed by [48, 10], we consider steady vortex solutions with a solenoidal velocity field

$$\mathbf{v}(x, y) = -h(\rho(x, y)) \begin{pmatrix} x - x_0 \\ y - y_0 \end{pmatrix}^\perp \quad (29)$$

with $\rho(x, y) = \|\mathbf{x} - \mathbf{x}_0\|$ and $h : \mathbb{R}^+ \rightarrow \mathbb{R}$. The pressure is obtained by solving $\nabla p = c \mathbf{v}^\perp = -c h(\rho(x, y))(\mathbf{x} - \mathbf{x}_0)$; using that $\rho \nabla \rho = \mathbf{x} - \mathbf{x}_0$ one finds

$$p(x, y) = P_0 - c g(\rho(x, y)) \quad (30)$$

with $g'(\rho) = \rho h(\rho)$ and $P_0 = \text{const.}$

2.2 Steady states with mass source only

In this case, we consider only a scalar source term $S_p \neq 0$ (that could, depending on the context, be called mass or pressure source). It leads to equilibria with a non-vanishing divergence:

$$\begin{cases} \text{div } \mathbf{v} = S_p, \\ p \equiv C \in \mathbb{R}, \end{cases} \quad (31)$$

which, using (16), becomes

$$\begin{cases} \mathcal{U} + \mathcal{V} - \mathcal{K}_p = \sigma^x(x) + \sigma^y(y), \\ p \equiv C \in \mathbb{R}. \end{cases} \quad (32)$$

Note the pressure is constant, due to the absence of sources in the velocity equations. We thus do not write compatibility relations for the boundary conditions in this case.

An example of the previous equilibrium can be obtained setting

$$\begin{cases} p(x, y) \equiv p_0, \\ \mathbf{v}(x, y) := -a h(\rho(x, y)) \begin{pmatrix} x - x_0 \\ y - y_0 \end{pmatrix}^\perp + b \nabla g(x, y), \\ S_p(x, y) := b \Delta g(x, y), \\ \mathbf{S}_v(x, y) := 0, \end{cases} \quad (33)$$

where $\rho(x, y) = \|\mathbf{x} - \mathbf{x}_0\|$, a and b are constants, and $g : \Omega \rightarrow \mathbb{R}$ and $h : \mathbb{R}^+ \rightarrow \mathbb{R}$ are sufficiently smooth functions.

We can easily modify the above problem to obtain a moving solution. This is useful for validation purposes. For example, given a constant vector $\mathbf{a} = (a_x, a_y) \in \mathbb{R}^2$, we can show that a translating solution is given by

$$\begin{cases} p(x, y) \equiv p_0 + b \mathbf{a} \cdot \nabla g(x - a_x t, y - a_y t), \\ \mathbf{v}(x, y) := a h(\rho(\mathbf{x} - \mathbf{x}_0(t))) (\mathbf{x} - \mathbf{x}_0(t))^\perp + b \nabla g(x - a_x t, y - a_y t), \\ S_p(x, y) := b \Delta g(x - a_x t, y - a_y t) - b \mathbf{a} \cdot \nabla (\mathbf{a} \cdot \nabla g), \\ \mathbf{S}_v(x, y) := 0, \end{cases} \quad (34)$$

with $\mathbf{x}_0(t) = (x_0 - a_x t, y_0 - a_y t)$.

2.3 Steady state with all velocity sources: the Stommel Gyre

We consider the general case in which all momentum sources are present, such that the steady state is governed by

$$\nabla \cdot \mathbf{v} = 0, \quad (35)$$

$$\nabla p = c(x, y) \mathbf{v}^\perp - f(x, y) \mathbf{v} + \boldsymbol{\tau}(x, y). \quad (36)$$

Integrating both components one obtains

$$\begin{aligned} p &= \int_{x_0}^x c v \, ds - \int_{x_0}^x f u \, ds + \int_{x_0}^x \tau_u \, ds + \sigma_u^y(y), \\ p &= - \int_{y_0}^y c u \, ds - \int_{y_0}^y f v \, ds + \int_{y_0}^y \tau_v \, ds + \sigma_v^y(x), \end{aligned}$$

where $\sigma_v^x = p(x, y_0)$, and $\sigma_u^y = p(x_0, y)$ are to be determined. To this end we evaluate the first above for $y = y_0$, and the second for $x = x_0$ to obtain the compatibility relations (as before $p_0 = p(x_0, y_0)$):

$$\begin{aligned} p(x_0, y) &= p_0 - \int_{y_0}^y (c u)(x_0, s) \, ds - \int_{y_0}^y f v(x_0, s) \, ds + \int_{y_0}^y \tau_v(x_0, s) \, ds, \\ p(x, y_0) &= p_0 + \int_{x_0}^x (c v)(s, y_0) \, ds - \int_{x_0}^x f u(s, y_0) \, ds + \int_{x_0}^x \tau_u(s, y_0) \, ds. \end{aligned} \quad (37)$$

Note that, unless c is constant, we cannot use the mass equation to couple the two expressions.

A classical example studied in meteorology is based on geostrophic shallow water equations, under a linearization assumption around the reference depth $h_0 = 1$ and with a re-scaling of gravity $g = 1$, the so-called Stommel Gyre model [51, 21]. The model is the acoustic system (2) with

- a Coriolis source term with the coefficient $c(x, y) := c_1 y + c_0$ (linear in the latitude y),
- a friction source term, where we use a constant $f \in \mathbb{R}^+$,
- a source in the velocity equations (wind forcing) in the form $\begin{cases} \tau_u = -F \cos(\pi y/b), \\ \tau_v = 0, \end{cases}$ with $F \in \mathbb{R}$ constant,
- no pressure source: $S_p = 0$.

A well-known particular steady state on the rectangular domain $\Omega = [0, \lambda] \times [0, b]$ is (see [51] for details):

$$\psi(x, y) = \gamma(b/\pi)^2 \sin(\pi y/b) (k e^{Ax} + w e^{Bx} - 1) \quad (38)$$

$$\begin{cases} u(x, y) = \partial_y \psi(x, y) = \gamma(b/\pi) \cos(\pi y/b) (k e^{Ax} + w e^{Bx} - 1), \\ v(x, y) = -\partial_x \psi(x, y) = -\gamma(b/\pi)^2 \sin(\pi y/b) (k A e^{Ax} + w B e^{Bx}), \end{cases} \quad \text{with } \begin{cases} \alpha = \frac{c_0}{f}, \\ \gamma = \frac{F\pi}{bf}, \end{cases} \quad (39)$$

with the coefficients k, w given by

$$k = \frac{1 - e^{B\lambda}}{e^{A\lambda} - e^{B\lambda}}, \quad w = 1 - k, \quad (40)$$

and A, B are the characteristic roots given by

$$\begin{aligned} A &= -\frac{\alpha}{2} + \sqrt{\frac{\alpha^2}{4} + (\pi/b)^2}, \quad A^2 = (\pi/b)^2 - \alpha A, \\ B &= -\frac{\alpha}{2} - \sqrt{\frac{\alpha^2}{4} + (\pi/b)^2}, \quad B^2 = (\pi/b)^2 - \alpha B. \end{aligned} \quad (41)$$

The steady pressure field can be expressed as

$$\begin{aligned} p &= -F \left(\frac{k}{A} e^{Ax} + \frac{w}{B} e^{Bx} \right) - F(b/\pi)^2 (kAe^{Ax} + wBe^{Bx}) (\cos(\pi y/b) - 1) \\ &\quad - \{c(x, y)\gamma(b/\pi)^2 \sin(\pi y/b) + \gamma c_0(b/\pi)^3 (\cos(\pi y/b) - 1)\} (ke^{Ax} + we^{Bx} - 1). \end{aligned} \quad (42)$$

This is a complex multi-dimensional case that couples all effects, and does not exhibit the same simple structure in terms of boundary conditions. The variability of the Coriolis coefficient makes it easier in practice to assume the velocities to be given on the boundaries, and look for compatible integration constants for the pressure.

3 Discrete setting: Finite Elements on Cartesian meshes

The discretization of hyperbolic equations with continuous Finite Element methods (FEM) requires some stabilization techniques. We focus here on the Streamline Upwind (SU) stabilization [30, 41, 42], and on the orthogonal sub-scale stabilization (OSS) [20, 19, 42]. For additional details on the spatial discretization of acoustic equations with stabilized continuous FEM we refer to [10].

3.1 Tensor-product Finite Element spaces

Let us consider a rectangular domain $\Omega := \Omega^x \times \Omega^y = [x_0, x_e] \times [y_0, y_e] \subset \mathbb{R}^2$ and a Cartesian mesh with cells $E_{ij} := E_i^x \times E_j^y := [x_i, x_{i+1}] \times [y_j, y_{j+1}]$ with $i = 0, \dots, N_x - 1, j = 0, \dots, N_y - 1, |E_i^x| = \Delta x, |E_j^y| = \Delta y$ and $h := \min(\Delta x, \Delta y)$. We define the numerical domains as $\Omega_{\Delta x}^x := \cup_{i=0}^{N_x-1} [x_i, x_{i+1}]$, $\Omega_{\Delta y}^y := \cup_{j=0}^{N_y-1} [y_j, y_{j+1}]$, and $\Omega_h := \cup_{i=0}^{N_x-1} \cup_{j=0}^{N_y-1} [x_i, x_{i+1}] \times [y_j, y_{j+1}]$. To be fully precise, since Ω is rectangular, $\Omega = \Omega_h$, so we will simply use Ω below.

We define continuous nodal FEM spaces of polynomial degree K by introducing $K + 1$ points in each one-dimensional cell $x_{i,p} \in E_i^x$, for $p = 0, \dots, K$, and $y_{j,\ell} \in E_j^y$, for $\ell = 0, \dots, K$. These points are used to define the Lagrangian basis functions. We will use Gauss-Lobatto points in each cell and $x_{i,0} = x_{i-1,K}$ for all $i = 1, N_x - 1$ and similarly for y , to obtain continuity all over the domain.

The relevant spaces over one/two-dimensional domains are

$$V_{\Delta x}^K(\Omega_{\Delta x}^x) := \{q \in \mathcal{C}^0(\Omega_{\Delta x}^x) : q|_E \in \mathbb{P}^K(E), \forall E \in \Omega_{\Delta x}^x\}, \quad (43a)$$

$$V_{\Delta y}^K(\Omega_{\Delta y}^y) := \{q \in \mathcal{C}^0(\Omega_{\Delta y}^y) : q|_E \in \mathbb{P}^K(E), \forall E \in \Omega_{\Delta y}^y\}, \quad (43b)$$

$$V_h^K(\Omega) := \{q \in \mathcal{C}^0(\Omega) : q|_E \in \mathbb{Q}^K(E), \forall E \in \Omega\}, \quad (43c)$$

where \mathbb{P}^K is the space of univariate polynomials of degree up to K , and \mathbb{Q}^K is the tensor product space of such polynomials in x and y directions. For simplicity we will occasionally write $V_{\Delta x} \equiv V_{\Delta x}^K(\Omega_{\Delta x}^x)$, $V_{\Delta y} \equiv V_{\Delta y}^K(\Omega_{\Delta y}^y)$, $V_h \equiv V_h^K(\Omega)$. In each one-dimensional cell E_i^x , we consider the Lagrangian basis functions $\varphi_{i,p}^x \in V_{\Delta x}$ such that $\varphi_{i,p}^x(x_{i,\ell}) = \delta_{p,\ell}$, the Kronecker delta, for every $p, \ell = 0, \dots, K$ and $i = 0, \dots, N_x - 1$. Moreover, since any $\varphi \in V_{\Delta x}$ must be continuous,

$$\text{supp}(\varphi_{i,p}^x) = E_i^x \text{ for } p = 1, \dots, K - 1, \quad \text{supp}(\varphi_{i,0}^x) = \text{supp}(\varphi_{i-1,K}^x) = E_{i-1}^x \cup E_i^x,$$

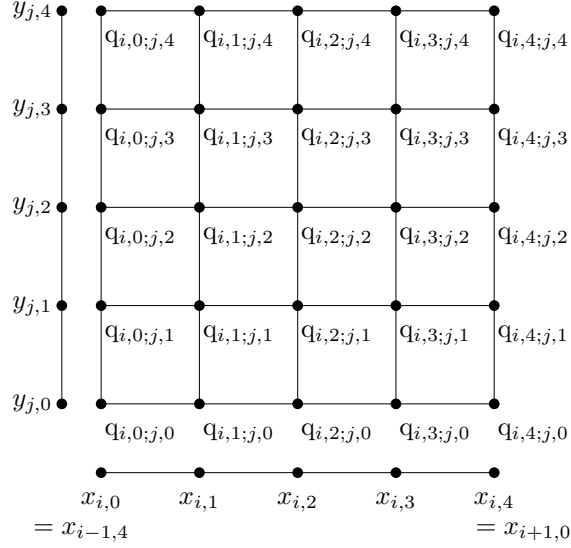


Figure 1: Notation of the degrees of freedom for a function q in element E_{ij} for \mathbb{Q}^4 elements

recalling that $\varphi_{i-1,K}^x = \varphi_{i,0}^x$. The same holds for the basis functions of the y space $\varphi_{j,\ell}^y$. Finally, the approximation space is $V_{\Delta x}^K(\Omega_{\Delta x}^x) = \text{span}\{\varphi_{i,p}^x\}_{i,p=0}^{N_x-1,K}$. We use the same spaces to discretize vector components as those we use for scalars.

This leads to the definition of V_h as a tensor product of the function spaces, with the basis $\varphi_{i,p;j,\ell}(x,y) := \varphi_{i,p}^x(x)\varphi_{j,\ell}^y(y)$ for $i = 0, \dots, N_x-1$, $j = 0, \dots, N_y-1$, $p, \ell = 0, \dots, K$. Finally, we will describe any function $q_h \in V_{\Delta x}$ having a uni-directional dependence on x as

$$q_h(x) = \sum_{i=0}^{N_x-1} \sum_{p=0}^K q_{i,p} \varphi_{i,p}^x|_{E_i^x}(x). \quad (44)$$

Note that the summation runs over $K+1$ nodes in each element $p \in \{0, \dots, K\}$, corresponding to a degree K interpolation, but $q_{i,0} = q_{i-1,K}$ for all $i = 1, \dots, N_x$. Similarly, a function $q_h \in V_h$ with dependence on both spatial variables is expanded as

$$q_h(x,y) = \sum_{i=0; j=0}^{N_x-1; N_y-1} \sum_{p=0; \ell=0}^{K; K} q_{i,p;j,\ell} \varphi_{i,p}^x(x)|_{E_i^x} \varphi_{j,\ell}^y(y)|_{E_j^y}, \quad (45)$$

with similar constraints on the degrees of freedom $q_{i,p;k,\ell}$. For periodic or homogeneous Dirichlet boundary conditions this can be written as

$$q_h(x,y) = \sum_{i=0; j=0}^{N_x-1; N_y-1} \sum_{p=1; \ell=1}^{K; K} q_{i,p;j,\ell} \varphi_{i,p}^x(x) \varphi_{j,\ell}^y(y) = \sum_{i=0; j=0}^{N_x-1; N_y-1} \sum_{p=1; \ell=1}^{K; K} q_{i,p;j,\ell} \varphi_{i,p;j,\ell}(x,y). \quad (46)$$

We will use the roman font q for the degrees of freedom that refer to a function $q_h \in V_h$ in a discrete Finite Element space. See Figure 1 for a graphical representation of degrees of freedom (DOFs) $q_{i,p;j,\ell}$ in a cell E_{ij} for $K = 4$.

3.2 Weak formulation

The unstabilized (central) continuous Galerkin weak form of the system (2) reads

$$\begin{cases} \int_{\Omega} \varphi (\partial_t u_h + \partial_x p_h - (S_u)_h) \, dx dy = 0, & \forall \varphi \in V_h^0, \\ \int_{\Omega} \varphi (\partial_t v_h + \partial_y p_h - (S_v)_h) \, dx dy = 0, & \forall \varphi \in V_h^0, \\ \int_{\Omega} \varphi (\partial_t p_h + \partial_x u_h + \partial_y v_h - (S_p)_h) \, dx dy = 0, & \forall \varphi \in V_h^0, \end{cases} \quad (47)$$

subject to suitable boundary conditions (BC), with $V_h^0 := \{\varphi \in V_h : \varphi(x, y) = 0 \text{ for } (x, y) \in \partial\Omega\}$.

Let us denote with Greek letters the tuples used for defining the one-dimensional basis functions, e.g. $\alpha = (i, p)$, and with $\mathcal{Q}^x := \{\alpha = (i, p) : 0 \leq i < N_x, 1 \leq p \leq K\}$ the set of all unique indices. Using the discretization of the variables as in (46), we can rewrite the central Galerkin discretization with one-dimensional matrices defined for all $\alpha, \beta \in \mathcal{Q}^x$ (similarly for \mathcal{Q}^y) as (see also [10] for a lengthier description)

$$\begin{aligned} (M_x)_{\alpha, \beta} &:= \int_{\Omega_x} \varphi_{\alpha}(x) \varphi_{\beta}(x) dx, & (D_x)_{\alpha, \beta} &:= \int_{\Omega_x} \varphi_{\alpha}(x) \frac{d}{dx} \varphi_{\beta}(x) dx, \\ (D_x^x)_{\alpha, \beta} &:= \int_{\Omega_x} \frac{d}{dx} \varphi_{\alpha}(x) \frac{d}{dx} \varphi_{\beta}(x) dx, & (D^x)_{\alpha, \beta} &:= \int_{\Omega_x} \frac{d}{dx} \varphi_{\alpha}(x) \varphi_{\beta}(x) dx. \end{aligned} \quad (48)$$

Using these operators, (47) becomes in a vectorial form

$$\begin{cases} M_x \otimes M_y \partial_t \mathbf{u} + D_x \otimes M_y \mathbf{p} - M_x \otimes M_y \mathbf{S}_u = 0, \\ M_x \otimes M_y \partial_t \mathbf{v} + M_x \otimes D_y \mathbf{p} - M_x \otimes M_y \mathbf{S}_v = 0, \\ M_x \otimes M_y \partial_t \mathbf{p} + D_x \otimes M_y \mathbf{u} + M_x \otimes D_y \mathbf{v} - M_x \otimes M_y \mathbf{S}_p = 0, \end{cases} \quad (49)$$

where \otimes denotes the Kronecker product between matrices and $\mathbf{u}, \mathbf{v}, \mathbf{p}, \mathbf{S}_u, \mathbf{S}_v, \mathbf{S}_p$ are the corresponding coefficients of the functions in V_h . For more details, see [10]. In practice, this might necessitate the evaluation of some source terms, e.g. $c(x, y)v_h(x, y)$ or $s_h^u(x, y)$ in the same Gauss–Lobatto quadrature points.

3.3 Stabilization approaches

For initial value problems, the Lax-Richtmyer stability of central collocated approximations as the Continuous Galerkin Finite Element methods can be shown under a Δx^2 time step constraint (see e.g. [36], chapter 10). Note that this stability criterion only guarantees the boundedness of the discrete solution, and is weaker than the usual Fourier (von Neumann) stability criterion requiring the norm of the complex amplification factor to be below 1.

For initial-boundary value problems this can be improved via appropriate treatments of the boundary conditions [2]. It is, however, generally accepted that central collocated methods require stabilization. Differently from methods using discontinuous data, we cannot introduce Riemann Problems and upwinding for stabilization. Thus, some stabilizing operator must be explicitly added to the variational equations. Below, we present two stabilization approaches that allow to use explicit time integration with CFL conditions, where Δt depends linearly on Δx .

3.3.1 Streamline upwind stabilization

We discuss here the Streamline-Upwind (SU) stabilization, leading to the well known SUPG (Streamline-Upwind Petrov-Galerkin) discretization [15, 30]. For our system the SU stabilization term reads

$$\mathcal{ST}_{\text{SU}}(\varphi, q_h = (u_h, v_h, p_h)) := \int_{\Omega} \alpha h (\partial_x \varphi J^x + \partial_y \varphi J^y) (\partial_t q_h + \nabla \cdot \mathbf{F}(q_h) - \mathbf{S}(q_h)) \, dx \, dy, \quad (50)$$

with J^x and J^y the Jacobian of the fluxes as in (4). The energy stability associated to this approach is discussed in a more general setting in appendix A.1. The stabilization terms added to each equation read

$$\begin{cases} \int_{\Omega} \alpha h \partial_x \varphi (\partial_t p_h + \partial_x u_h + \partial_y v_h - (S_p)_h) \, dx dy, \\ \int_{\Omega} \alpha h \partial_y \varphi (\partial_t p_h + \partial_x u_h + \partial_y v_h - (S_p)_h) \, dx dy, \\ \int_{\Omega} \alpha h [\partial_x \varphi (\partial_t u_h + \partial_x p_h - (S_u)_h) + \partial_y \varphi (\partial_t v_h + \partial_y p_h - (S_v)_h)] \, dx dy, \end{cases} \quad (51)$$

or, in vectorial form,

$$\begin{cases} \alpha h (D^x \otimes M_y \partial_t \mathbf{p} + D_x^x \otimes M_y \mathbf{u} + D^x \otimes D_y \mathbf{v} - D^x \otimes M_y \mathbf{S}_p), \\ \alpha h (M_x \otimes D^y \partial_t \mathbf{p} + D_x \otimes D^y \mathbf{u} + M_x \otimes D_y^y \mathbf{v} - M_x \otimes D^y \mathbf{S}_p), \\ \alpha h (D^x \otimes M_y \partial_t \mathbf{u} + D_x^x \otimes M_y \mathbf{p} - D^x \otimes M_y \mathbf{S}_u) + \\ \alpha h (M_x \otimes D^y \partial_t \mathbf{v} + M_x \otimes D_y^y \mathbf{p} - M_x \otimes D^y \mathbf{S}_v). \end{cases} \quad (52)$$

An explicit time discretization of this method will be discussed in section 6. The spectral stability of this approach using several explicit time-discretization methods is studied in [41, 42].

Remark 1 (Streamline upwinding and steady state preservation). *Being a residual based stabilization, and involving grad(div) type terms, the SU stabilization approach has in principle all the desired features to preserve moving equilibria. Unfortunately, as shown in [10], the SUPG scheme is not stationary preserving because the discrete Galerkin variational form and the streamline upwind stabilization operator have different kernels, which do not include the same discrete approximation of the physical steady state [10]. This ultimately leads to the dissipation of steady states, which can only be preserved within the accuracy of the method, thus on sufficiently fine meshes and for short simulation times.*

3.3.2 Orthogonal Sub-scale stabilization (OSS)

The Orthogonal Sub-scale Stabilization (OSS) adds a penalty term on the weak derivative of the residual. It was originally presented for Stokes equation [20], then for convection–diffusion–reaction problems [19, 7] and for hyperbolic problems [41, 42]. A multi-dimensional steady state compliant version of this method for homogeneous problems has been proposed already in [10]. For our system, it can be written as

$$\begin{aligned} & \int_{\Omega} \alpha h \partial_x \varphi (\nabla \cdot \mathbf{v}_h - (S_p)_h - w^{\nabla \cdot \mathbf{v}}) \, dx dy, \\ & \int_{\Omega} \alpha h \partial_y \varphi (\nabla \cdot \mathbf{v}_h - (S_p)_h - w^{\nabla \cdot \mathbf{v}}) \, dx dy, \\ & \int_{\Omega} \alpha h \partial_x \varphi (\partial_x p_h - (S_u)_h - w^{\partial_x p}) \, dx dy + \int_{\Omega} \alpha h \partial_y \varphi (\partial_y p_h - (S_v)_h - w^{\partial_y p}) \, dx dy, \end{aligned} \quad (53)$$

with the L^2 projections $w^{\nabla \cdot \mathbf{v}}$, $w^{\partial_x p}$ and $w^{\partial_y p}$ defined by

$$\int_{\Omega} \varphi (w^{\nabla \cdot \mathbf{v}} - (\nabla \cdot \mathbf{v}_h - (S_p)_h)) = 0, \quad (54)$$

$$\int_{\Omega} \varphi (w^{\partial_x p} - (\partial_x p_h - (S_u)_h)) = 0, \quad (55)$$

$$\int_{\Omega} \varphi (w^{\partial_y p} - (\partial_y p_h - (S_v)_h)) = 0. \quad (56)$$

By construction, the terms of the form $\partial_x p_h - (S_u)_h - w^{\partial_x p}$ are not zero and introduce L^2 stabilization. The energy stability associated to this approach is discussed in a more general setting in appendix A.2. See also [19, 7, 41, 42, 10] for more details. The OSS operator can also be cast in compact matrix form. Computations show that several terms cancel out. For example, for the first term we have that

$$\mathbf{w}^{\nabla \cdot \mathbf{v}} := (M_x^{-1} \otimes M_y^{-1}) [D_x \otimes M_y \mathbf{u} + M_x \otimes D_y \mathbf{v} - M_x \otimes M_y \mathbf{S}_p]$$

and

$$\begin{aligned} & \alpha h \left(D_x^x \otimes M_y u - D^x M_x^{-1} D_x \otimes M_y u + \cancel{D^x \otimes D_y v} - \cancel{D^x \otimes D_y v} + \cancel{D^x \otimes M_y S_p} - \cancel{D^x \otimes M_y S_p} \right) \\ & = \alpha h (D_x^x - D^x M_x^{-1} D_x) \otimes M_y u. \end{aligned}$$

Proceeding similarly for all terms, we obtain the compact expressions

$$\begin{cases} \alpha h Z_x \otimes M_y u, \\ \alpha h M_x \otimes Z_y v, \\ \alpha h (Z_x \otimes M_y p + M_x \otimes Z_y p), \end{cases} \quad (57)$$

having defined the matrices

$$Z_x := D_x^x - D^x M_x^{-1} D_x, \quad Z_y := D_y^y - D^y M_y^{-1} D_y. \quad (58)$$

All the differences between sources and their projection cancel out in the stabilization terms, as shown in the first equation. This will not be the case in the multi-dimensional GF well-balanced formulation discussed later. We refer to [41, 42] for a study of the spectral stability of this approach with several explicit time-discretization methods.

Remark 2 (OSS and steady state preservation). *The OSS is based on the approximation of $\text{grad}(\text{div})$ stabilization terms and it is a good candidate for stationarity preservation. However, similarly to SUPG, in [10] the authors show that in its standard formulation the OSS method is not stationarity preserving. It thus requires sufficiently fine meshes to appropriately resolve multi-dimensional steady states. As for SUPG, this is related to the difference in the kernels of the discrete Galerkin variational form and of the stabilization operator. We refer to [10] for details.*

4 Multidimensional Global Flux formulation

We now modify the discrete variational form (47) by incorporating the multi-dimensional GF approach, which follows the ideas of Section 1.2. As in [10], we will

1. define a modified variational form whose kernel contains an appropriate discrete notion of steady state;
2. characterize the discrete steady state by obtaining a pointwise error estimation w.r.t. the physical/exact steady solution;
3. define a modification of the stabilization operators consistent with the same steady state.

The nature of the discrete steady state introduced in 1 is such that it is possible (in 3) to find a stabilization operator with the same steady state, something not possible otherwise. As we will see, our approach allows to obtain methods with physically relevant discrete stationary states, which can be precisely characterized. However, these steady states are not point-wise exact approximations. For stationarity preserving schemes point-wise evaluations of the stationary states of the PDE will in general develop some small amplitude initial layer before settling down onto the numerical steady state, which is a good approximation of the exact one (if the boundary conditions are appropriately set). Stationarity preserving methods outperform in any case the standard ones which generally dissipate all but the simplest equilibria.

If one is interested in simulations of very small perturbations, we need to ensure the absence of any initial layer, i.e., that the discrete data are well-prepared with respect to the discrete equilibria of the method. In this case, we need to add to the above list:

4. an initialization procedure that projects data on the discrete kernel.

We will discuss all these aspects in this section, except the modification of the stabilization terms that will be defined in Section 5.

4.1 Variational form using Global Flux quadrature

Our starting point is the formulation (15) of section 1.2:

$$\begin{cases} \partial_t u + \partial_x(p - \mathcal{K}_u) = 0, \\ \partial_t v + \partial_y(p - \mathcal{K}_v) = 0, \\ \partial_t p + \partial_{xy} G_p = 0. \end{cases}$$

As already remarked, in the first two equations, a one-dimensional GF formulation is applied, while in the last equation we present a genuinely multi-dimensional GF approach. Similar results can be obtained by treating the gradient as the divergence of a diagonal tensor.

To achieve a discretization of (15), we need to define discrete counterparts of the integrated variables \mathcal{U} , \mathcal{V} , \mathcal{K}_p and \mathcal{K}_v introduced in (11) and (14). Following [38, 10], we will approximate these variables in the same polynomial space as the actual unknowns, i.e., with the notation of (45),

$$\begin{aligned} \mathcal{U}_h &= \sum_{i=0; j=0}^{N_x-1; N_y-1} \sum_{p=0; \ell=0}^{K; K} U_{i,p;j,\ell} \varphi_{i,p}^x(x) |_{E_i^x} \varphi_{j,\ell}^y(y) |_{E_j^y}, \\ \mathcal{V}_h &= \sum_{i=0; j=0}^{N_x-1; N_y-1} \sum_{p=0; \ell=0}^{K; K} V_{i,p;j,\ell} \varphi_{i,p}^x(x) |_{E_i^x} \varphi_{j,\ell}^y(y) |_{E_j^y}, \\ (\mathcal{K}_v)_h &= \sum_{i=0; j=0}^{N_x-1; N_y-1} \sum_{p=0; \ell=0}^{K; K} (\mathbf{K}_v)_{i,p;j,\ell} \varphi_{i,p}^x(x) |_{E_i^x} \varphi_{j,\ell}^y(y) |_{E_j^y}, \\ (\mathcal{K}_p)_h &= \sum_{i=0; j=0}^{N_x-1; N_y-1} \sum_{p=0; \ell=0}^{K; K} (K_p)_{i,p;j,\ell} \varphi_{i,p}^x(x) |_{E_i^x} \varphi_{j,\ell}^y(y) |_{E_j^y}. \end{aligned} \tag{59}$$

We need to define the coefficients $U_{i,p;j,\ell}$, $V_{i,p;j,\ell}$, $(\mathbf{K}_v)_{i,p;j,\ell}$, and $(K_p)_{i,p;j,\ell}$. To this end, in each cell $E_{ij} := E_i^x \times E_j^y$ we set (we simplify the notation by avoiding the restriction to the elements which is clear from the context)

$$\begin{aligned} U_{i,p;j,\ell} &= U_{i,p;j,0} + \int_{y_{j,0}}^{y_{j,\ell}} u_h(x_{i,p}, y) dy = U_{i,p;j,0} + \sum_{n=0}^K u_{i,p;j,n} \int_{y_{j,0}}^{y_{j,\ell}} \varphi_{j,n}^y(y) dy, \quad \ell = 1, \dots, K, \forall p, \\ V_{i,p;j,\ell} &= V_{i,0;j,\ell} + \int_{x_{i,0}}^{x_{i,p}} v_h(x, y_{j,\ell}) dx = V_{i,0;j,\ell} + \sum_{m=0}^K v_{i,m;j,\ell} \int_{x_{i,0}}^{x_{i,p}} \varphi_{i,m}^x(x) dx, \quad p = 1, \dots, K, \forall \ell, \\ (K_p)_{i,p;j,\ell} &= (K_p)_{i,0;j,0} + \int_{x_{i,0}}^{x_{i,p}} \int_{y_{j,0}}^{y_{j,\ell}} (S_p)_h(x, y) dy dx \\ &= (K_p)_{i,0;j,0} + \sum_{m=0; n=0}^{K; K} (S_p)_{i,m;j,n} \int_{x_{i,0}}^{x_{i,p}} \varphi_{i,m}^x(x) dx \int_{y_{j,0}}^{y_{j,\ell}} \varphi_{j,n}^y(y) dy \quad (p, \ell) \in \{0, \dots, p\}^2 \setminus (0, 0), \end{aligned} \tag{60}$$

for all $i = 0, \dots, N_x - 1$ and $j = 0, \dots, N_y - 1$. The above relations define summations along grid lines. We are left to define the interface values, which can be found imposing continuity as

$$U_{i,p;j,0} := U_{i,p;j-1,K} \quad \text{for all } i = 0, \dots, N_x - 1, j = 1, \dots, N_y - 1, p = 0, \dots, K, \tag{61}$$

$$V_{i,0;j,\ell} := V_{i-1,K;j,\ell} \quad \text{for all } i = 1, \dots, N_x - 1, j = 0, \dots, N_y - 1, \ell = 0, \dots, K, \tag{62}$$

$$(K_p)_{i,0;j,0} := (K_p)_{i-1,K;j-1,K} \quad \text{for all } i = 1, \dots, N_x - 1, j = 1, \dots, N_y - 1. \tag{63}$$

The remaining boundary values can be set to 0 [38], as the integral is defined up to a constant. The value of these integrated quantities is not so relevant as the integral operators will always be paired with

a derivative operator. Hence, only their difference with respect to the border of the cell will be relevant. This means that only (60) will be relevant for the actual method.

The definitions of the components of $(\mathbf{K}_v)_{i,p;j,\ell}$ are analogous to those of $V_{i,p;j,\ell}$ for $(\mathbf{K}_u)_{i,p;j,\ell}$, and of $U_{i,p;j,\ell}$ for $(\mathbf{K}_v)_{i,p;j,\ell}$. The above relations define summations along grid lines. The initial states in these summations are obtained imposing continuity across elements. In other words we have $U_{i,p;j,0} = U_{i,p;j-1,K}$, $V_{i,0;j,\ell} = V_{i-1,K;j,\ell}$ and similarly for all the others. After assembly, all these quantities are defined up to arrays containing constant entries, which will not affect the final discretization. For this reason, these global integration constants are simply taken equal to zero as in [38].

All the above computations can be re-written through two local linear operators that we denote by one-dimensional matrices I_x and I_y , defined as

$$(I_x)_{i_1,p_1;i_2,p_2} := \int_{x_{i_1,0}}^{x_{i_1,p_1}} \varphi_{i_2,p_2}^x(x) dx, \quad (I_y)_{j_1,p_1;j_2,p_2} := \int_{y_{j_1,0}}^{y_{j_1,\ell_1}} \varphi_{j_2,\ell_2}^y(y) dy. \quad (64)$$

In this way, we can define the discrete GF variables as

$$U = \mathbb{1}_x \otimes I_y u, \quad V = I_x \otimes \mathbb{1}_y v, \quad K_u = I_x \otimes \mathbb{1}_y S_u, \quad K_v = \mathbb{1}_x \otimes I_y S_v, \quad K_p = I_x \otimes I_y S_p, \quad (65)$$

with $\mathbb{1}_x$ and $\mathbb{1}_y$ being the identity matrices. As noted in [38, 10], when using Gauss-Lobatto interpolation points the local operators I_x and I_y are by definition the Butcher tableaux of the well known LobattoIIIA collocation method for ODE integration [29]. This is important for the consistency analysis below.

Discrete equations are now obtained using the Galerkin projection (15). The resulting (unstabilized central) discrete variational equations read as follows

$$\begin{cases} M_x \otimes M_y \partial_t u + D_x \otimes M_y p - D_x I_x \otimes M_y S_u = 0, \\ M_x \otimes M_y \partial_t v + M_x \otimes D_y p - M_x \otimes D_y I_y S_v = 0, \\ M_x \otimes M_y \partial_t p + D_x \otimes D_y I_y u + D_x I_x \otimes D_y v - D_x I_x \otimes D_y I_y S_p = 0. \end{cases} \quad (66a)$$

Note that the quantity $D_x \otimes D_y I_y u + D_x I_x \otimes D_y v$ in the last equation is exactly the GF DIV operator introduced in [10]. Here, we additionally account for the source terms in a multi-dimensional fashion. Furthermore, we can factor out the differential operators in all the evolution terms as

$$\begin{cases} R_c^u(u, v, p) := M_x \otimes M_y \partial_t u + D_x \otimes M_y (p - I_x \otimes \mathbb{1}_y S_u) = 0, \\ R_c^v(u, v, p) := M_x \otimes M_y \partial_t v + M_x \otimes D_y (p - \mathbb{1}_x \otimes I_y S_v) = 0, \\ R_c^p(u, v, p) := M_x \otimes M_y \partial_t p + D_x \otimes D_y (\mathbb{1}_x \otimes I_y u + I_x \otimes \mathbb{1}_y v - I_x \otimes I_y S_p) = 0. \end{cases} \quad (66b)$$

This is the key to being able to later define a stabilization that does not destroy the stationary state.

Remark 3 (Symmetry of the GF quadrature). *Definitions (60) involve integrating, and marching in the positive direction of the reference axes in an element wise manner. This may lead that the conclusion that the resulting method has a directional dependence. This is in fact not true, and one easily checks that the same method is obtained when (60) are reversed and integration is started from the end points. This has been shown in detail in Proposition 9 of [10, section §4.3, page 13], and is briefly recalled for completeness. Consider for example the reversed variable*

$$\tilde{V}_{i,p;j,\ell} := \tilde{V}_{i,K;j,\ell} + \int_{x_{i,K}}^{x_{i,p}} v(s, y_{j,\ell}) ds.$$

We can easily show that

$$\tilde{V}_{i,p;j,\ell} = V_{i,p;j,\ell} + \Delta_{i;j,\ell}^V, \quad \Delta_{i;j,\ell}^V := \tilde{V}_{i,K;j,\ell} - \tilde{V}_{i,0;j,\ell} - \int_{x_{i,0}}^{x_{i,K}} v(s, y_{j,\ell}) ds$$

with $V_{i,p;j,\ell}$ defined in (60). The quantity $\Delta_{i;j,\ell}^V$ is the same for all nodes, and as a consequence we have on any E_{ij}

$$\partial_x \tilde{V}_h = \partial_x V \quad \Rightarrow \quad D_x \otimes D_y \tilde{V} = D_x \otimes D_y V.$$

Similar developments can be performed for all the variables involved in (60), and in the variational form (66b). This shows that the GF quadrature formulation is symmetric and independent of the constants dropped. We refer to [10] for more.

Example 4 (GF \mathbb{Q}^1 operators). *The main difference with the classical Finite Element method discussed in section 3.2 is the replacement (in the divergence and source integral) of the mass matrices by the operators $D_x I_x$ and similarly in y . We can compare the resulting expressions (in x -direction) at lowest order of accuracy, where they can be written as finite differences (note that the integrals are computed with the same Gauss–Lobatto quadrature defining the basis functions, hence, the mass matrix is not exact):*

- *continuous Finite Element method:*
 $M_x \simeq (0, 1, 0), \quad D_x \simeq (-\frac{1}{2}, 0, \frac{1}{2}), \quad D^x \simeq (\frac{1}{2}, 0, -\frac{1}{2}), \quad D_x^x \simeq (-1, 2, -1);$
- *GF Finite Element method:* $I_x = \begin{pmatrix} 0 & 0 \\ \frac{1}{2} & \frac{1}{2} \end{pmatrix}$, so e.g.,

$$\mathcal{V}_h(x_{i+1}, y_j) = \mathcal{V}_h(x_i, y_j) + \frac{1}{2} (v_h(x_i, y_j) + v_h(x_{i+1}, y_j)).$$

This results in $D_x I_x = (\frac{1}{4}, \frac{1}{2}, \frac{1}{4})$ (new mass matrix), $D_x^x I_x = (\frac{1}{2}, 0, -\frac{1}{2}) = D^x$. As has been shown in [10], at lowest order the GF approach yields Finite Differences that appear in stationarity preserving methods for linear acoustics such as [45]. This is in particular true for the coefficients $(\frac{1}{4}, \frac{1}{2}, \frac{1}{4})$ of the “mass matrix” $D_x I_x$.

4.2 Discrete equilibria and super-convergence

In this section, we aim at characterizing explicitly the discrete steady states of the GF variational form (66b), and at analyzing their consistency with the steady states of the PDE.

4.2.1 Characterization of the discrete steady states

Proposition 5 (Discrete steady states of the GF discretization). *Equations (66) obtained from the GF formulation (15) of (2) admit the discrete steady states characterized by*

$$\begin{aligned} p_{i,k;j,s} - (K_u)_{i,k;j,s} &= \sigma_u^y(j, s), \\ p_{i,k;j,s} - (K_v)_{i,k;j,s} &= \sigma_v^x(i, k), \\ u_{i,k;j,s} + v_{i,k;j,s} - (K_p)_{i,k;j,s} &= \sigma_p^x(i, k) + \sigma_p^y(j, s). \end{aligned} \tag{67}$$

where σ_u^y, σ_p^y are arbitrary functions of j, s (y -direction), and σ_v^x, σ_p^x arbitrary functions of i, k (x -direction) only.

Proof. By construction $D_x \otimes D_y(\sigma_p^x + \sigma_p^y) = 0$ as $D_y \sigma_p^x = 0$ and $D_x \sigma_p^y = 0$, and similarly $D_x \sigma_u^y = 0$ and $D_y \sigma_v^x = 0$. Thus, the data (67) is in the kernel of the spatial operator of (66). \square

The above result provides a global representation of the discrete steady states. A more local description of these states can be obtained as follows. Consider the local assembly

$$[D_x \otimes D_y(U + V - K_p)]_{\alpha;\beta} = \sum_{E \ni (\alpha;\beta)} [D_x^E \otimes D_y^E ((\mathbb{1}_x^E \otimes I_y^E) u^E + (I_x^E \otimes \mathbb{1}_y^E) v^E - (I_x^E \otimes I_y^E) S_p^E)]_{\alpha;\beta},$$

where the superscript E denotes the local operators and arrays in a generic element E containing the point (α, β) , e.g. $(D_x^E)_{\alpha_1, \alpha_2} := \int_{E^x} \varphi_{\alpha_1}^x(x) \frac{d}{dx} \varphi_{\alpha_2}^x(x) dx$. Let us now focus on element $E = E_{ij}$, and consider the local arrays

$$[u_0^E]_{i,s;j,p} := u_{i,0;j,p} \quad \forall s = 0, \dots, K, \quad [v_0^E]_{i,s;j,p} := v_{i,s;j,0} \quad \forall p = 0, \dots, K.$$

Using the fact that $D_x^E \otimes \mathbb{1}_y^E u_0^E = \mathbb{1}_x^E \otimes D_y^E v_0^E = 0$, we can immediately write

$$[D_x \otimes D_y (U + V - K_p)]_{\alpha;\beta} = \sum_{E \ni (\alpha;\beta)} [(D_x^E \otimes D_y^E) \Phi_p^E]_{\alpha;\beta},$$

where Φ_p^E is the array of integrated residuals

$$\Phi_p^E := (\mathbb{1}_x^E \otimes I_y^E)(u^E - u_0^E) + (I_x^E \otimes \mathbb{1}_y^E)(v^E - v_0^E) - (I_x^E \otimes I_y^E S_p^E), \quad (68)$$

whose entries are readily shown to be given by

$$\begin{aligned} [\Phi_p^E]_{i,s;j,t} &= \int_{y_{j,0}}^{y_{j,t}} (u_h(x_{i,s}, y) - u_h(x_{i,0}, y)) dy + \int_{x_{i,0}}^{x_{i,s}} (v_h(x, y_{j,t}) - v_h(x, y_{j,0})) dx - \int_{x_{i,0}}^{x_{i,s}} \int_{y_{j,0}}^{y_{j,t}} (S_p)_h dx dy \\ &= \int_{x_{i,0}}^{x_{i,s}} \int_{y_{j,0}}^{y_{j,t}} (\partial_x u_h + \partial_y v_h - (S_p)_h) dx dy. \end{aligned} \quad (69)$$

In a similar manner, we can easily show that

$$\begin{aligned} [D_x \otimes \mathbb{1}_y (p - K_u)]_{\alpha;\beta} &= \sum_{E \ni (\alpha;\beta)} [D_x^E \otimes \mathbb{1}_y^E \Phi_u^E]_{\alpha;\beta}, \quad [\Phi_u^E]_{i,s;j,t} = \int_{x_{i,0}}^{x_{i,s}} (\partial_x p_h - (S_u)_h)(x, y_{j,t}) dx, \\ [\mathbb{1}_x \otimes D_y (p - K_v)]_{\alpha;\beta} &= \sum_{E \ni (\alpha;\beta)} [\mathbb{1}_x^E \otimes D_y^E \Phi_v^E]_{\alpha;\beta}, \quad [\Phi_v^E]_{i,s;j,t} = \int_{y_{j,0}}^{y_{j,t}} (\partial_y p_h - (S_v)_h)(x_{i,s}, y) dy. \end{aligned} \quad (70)$$

If now we consider the *residual vector*

$$\Phi^E = (\Phi_u^E, \Phi_v^E, \Phi_p^E)^t, \quad (71)$$

the components $(i, s; j, t)$ of Φ^E are integrals of the steady state residual, over sub-cells $[y_{i,0}, y_{i,t}]$, $[x_{i,0}, x_{i,s}]$, and $[x_{i,0}, x_{i,s}] \times [y_{i,0}, y_{i,t}]$ respectively. We can now reformulate the discrete steady states as follows.

Proposition 6 (Discrete steady states of the GF equations and vanishing subcell integrals). *The GF quadrature variational equations (66) admit the discrete steady states characterized by the condition*

$$\Phi_{i,s;j,t}^E = 0 \quad \forall s, t \text{ and } \forall E_{i,j}, \quad (72)$$

where Φ^E are the arrays of sub-cell integrated residuals (69), (70) and (71).

Several remarks are in order:

1. *From collocated to face averaged data.* The proposed multi-dimensional GF approach introduces a link between a collocated representation based on nodal values, and mimetic approaches based on face-averaged and cell-averaged quantities. The variables \mathcal{U}_h , \mathcal{V}_h are integrated values of the velocities in the directions normal to the faces, Similarly, $(K_p)_h$ is a sub-cell averaged term times a cell volume. These are natural objects to express integrals of the form

$$\begin{aligned} \iint (\partial_x u + \partial_y v - S_p) dx dy &= \int [u]_x dy + \int [v]_y dx - \iint S_p dx dy \\ &= \left[\int u dy \right]_x + \left[\int v dx \right]_y - \iint S_p dx dy, \end{aligned} \quad (73)$$

which characterize the steady state. The concepts generalize naturally to 3 space dimensions.

2. *Vanishing residuals.* Characterization (72) of the steady states is fully local to an element, and involves in principle as many conditions as the number of nodes in the mesh. However, one easily checks that there are at most $3 \times K^2 \times (N_x \times N_y) + K(N_x + N_y)$ independent conditions, for the system under consideration. These can be obtained on each element from the integrals on the smallest sub-quadrilaterals (and 1D sub-cells) defined by the Gauss-Lobatto points. The remaining ones can be obtained as sum of these integrals. These conditions characterize the dimension of kernel of the methods proposed. This residual property somewhat generalizes the steady state preserving properties of previously developed residual distribution methods [47, 22, 3, 4].
3. *Number of boundary conditions.* The total number of nodal unknowns when using an interpolation degree K is $3 \times (1 + KN_x) \times (1 + KN_y)$ for the system under consideration. Assuming that the number of equations obtained from the vanishing residuals condition are independent, then a unique equilibrium state would be determined by imposing at least $3 \times (1 + KN_x) \times (1 + KN_y) - 3 \times K^2 \times (N_x \times N_y) - K(N_x + N_y)$ boundary values. This is still often not the case, as (72) gives often redundant conditions, which makes this number of boundary conditions only a lower bound to characterize an equilibrium. In practice, the conditions imposed depend for each problem on the data actually available on each boundary.

4.2.2 Consistency analysis

The next step is to provide consistency estimates of the discrete equilibria identified above. To this end, we need to improve and generalize the nodal consistency argument given in [10].

Proposition 7 (Nodal super-convergence and line-by-line/row-by-row projection). *On a Cartesian domain $\Omega = [x_0, x_e] \times [y_0, y_e]$, consider a steady state solution composed of a vector field $\mathbf{v}_e = (u_e, v_e)$ and a pressure p_e with sufficient regularity, say $u_e, v_e, p_e \in C^P(\Omega)$ with P large enough. Assume that (\mathbf{v}_e, p_e) satisfy*

$$\begin{aligned}\partial_x p_e(x, y) &= S_u(\mathbf{v}_e, p_e; x, y), \\ \partial_y p_e(x, y) &= S_v(\mathbf{v}_e, p_e; x, y), \\ \partial_x u_e(x, y) + \partial_y v_e(x, y) &= S_p(x, y),\end{aligned}$$

at every point in space, and in particular at all collocation points. Let $(\mathbf{v}_e^\partial, p_e^\partial) = (\mathbf{v}_e, p_e)_{\partial\Omega}$ denote the boundary values of the steady solution. Given an ODE $U'(t) = F(U, t)$, let us consider multi-stage integrators

$$U_k - U_0 = (I_x F)_k, \quad U_k - U_0 = (I_y F)_k, \quad (74)$$

which are exact when F is a polynomial of degree M , also for an intermediate stage k . Then, there exists a discrete projection $(\mathbf{v}_e, p_e)_h$ of the exact solution on the discrete Finite Element space such that

- the order of accuracy of the projection only depends on the accuracy of the integrators, in particular we have $(\mathbf{v}_e, p_e)_h = (\mathbf{v}_e, p_e) + \mathcal{O}(h^M)$;
- there exist order $\mathcal{O}(h^M)$ perturbed boundary values $(\tilde{\mathbf{v}}_e^\partial, \tilde{p}_e^\partial) = (\mathbf{v}_e, p_e)_{\partial\Omega} + \mathcal{O}(h^M)$, such that $(\mathbf{v}_e, p_e)_h$ is in the kernel of the GF variational form (66a), and in particular it verifies Propositions 5 and 6, with $(\mathbf{v}_e, p_e)_h|_{\partial\Omega} = (\tilde{\mathbf{v}}_e^\partial, \tilde{p}_e^\partial)$ and with $(u_e)_h|_{\partial\Omega} = u_e^\partial$, $(v_e)_h|_{\partial\Omega} = v_e^\partial$, $(p_e)_h|_{\partial\Omega} = p_e^\partial$ holding true on at least one of the four sides of $\partial\Omega$ for each variable;
- the GF variational formulation using Gauss-Lobatto points admits super-convergent discrete steady states verifying the error estimate of order $\mathcal{O}(h^M)$ with $M = K + 2$ for polynomial interpolation of degree $K \geq 2$.

Proof. See Appendix B. □

We would like to make several remarks. One is that the accuracy of the integrators M is not necessarily related to the polynomial degree of the finite element space. Examples using multi-step-like procedures

with accuracy independent on the polynomial representation are provided in the finite-volume context in [34]. Similar approaches are possible in the Finite Element setting and will be explored in the future. Second, as already remarked, boundary conditions play a fundamental role in the definition of the discrete steady states. This is especially true when accounting for the presence of sources, which make the use of homogeneous or periodic boundary conditions not always suitable.

The above proposition and its proof provide two important elements. The first message is that, even if one does not use well prepared initial data, the discrete solution will settle, after some short transient, on a discrete steady state that has accuracy h^M everywhere, including on the boundaries. The numerical results reported in section 7 provide examples of this. Secondly, the proof is based on a constructive approach that explicitly introduces a projection of exact steady states onto the kernel of the scheme. This projection is based on a line-by-line/row-by-row integration method. This method, which is recalled in more detail the next section (see also Appendix B), provides at least one way of constructing well prepared data that are exactly preserved by the scheme. This is very useful when studying the evolution of very small perturbations. The next section gives a more in depth discussion on other approaches to obtain well prepared data.

4.2.3 Projections and well prepared initial data in practice

We discuss ways of obtaining well-prepared data. In this case, we are given a steady state of the PDE and aim at obtaining discrete data which are a steady state of the numerical method, and verify the accuracy estimate of proposition 7.

A first approach to achieve this objective is constructed in the proof of proposition 7 (see Appendix B). It consists of line-by-line/row-by-row iterations exploiting the integration tables I_x and I_y . Given boundary data $\tilde{u}(x_0, y)$, $\tilde{v}(x, y_0)$, and $\tilde{p}(x_0, y_0)$, it boils down to evaluating nodal values of the unknowns from the integrals

$$\begin{aligned} u(x, y) &= \tilde{u}(x_0, y) - \int_{x_0}^x (\partial_x u_e)_h(s, y) ds \\ v(x, y) &= \tilde{v}(x, y_0) - \int_{y_0}^y (\partial_y v_e)_h(x, s) ds \\ p(x, y) &= \tilde{p}(x_0, y_0) + (1 - \lambda) \left(\int_{x_0}^x (\partial_x p_e)_h(s, y_0) ds + \int_{y_0}^y (\partial_y p_e)_h(x, s) ds \right) \\ &\quad + \lambda \left(\int_{y_0}^y (\partial_y p_e)_h(x_0, s) ds + \int_{x_0}^x (\partial_x p_e)_h(s, y) ds \right) \end{aligned} \tag{75}$$

with $\lambda \in \mathbb{R}$ arbitrary, and having denoted by $(\partial_x u_e)_h$ the Lagrange interpolant on the Gauss-Lobatto points of the partial derivative of the exact velocity, and similarly for the other quantities. As shown in Appendix B the discrete data (75) above provide a projection of an exact stationary solution of the PDE into the kernel of the scheme. They satisfy the consistency estimates of the proposition. In [10] the above projection was called line-by-line/row-by-row (LobattoIIIA) projection (when the integrator tables are those obtained from the Gauss-Lobatto collocation points).

The directional line-by-line integration can be easily set up and provides quite satisfactory results. Unfortunately, it relies on the correct definition of the initial values on a specific boundary, and a choice of the integration direction. It thus introduces an asymmetry in the error of the initial data with respect to the exact one. This lack of symmetry is in contrast with the symmetry property of the GF quadrature recalled in Remark 3. To improve on this, one could imagine some iterative correction combining ODE integration in opposite directions.

A more efficient approach, used here, is to obtain well-prepared data using a projection based on a global optimization. Compared to the homogeneous case [10], here we need to account for the complexity introduced by the forcing terms both in the PDE and in the boundary conditions. Given an initial steady state (\mathbf{v}_0, p_0) , we first compute the nodal components of the velocity as

$$\arg \min_{\mathbf{u}, \mathbf{v} \in \mathcal{C}} (\|\mathbf{u} - \mathbf{u}_0\|^2 + \|\mathbf{v} - \mathbf{v}_0\|^2), \quad \mathcal{C} := \{\mathbf{u}, \mathbf{v} : D_x \otimes D_y I_y \mathbf{u} + D_x I_x \otimes D_y \mathbf{v} = \mathbf{S}_p\}, \tag{76a}$$

where u_0, v_0 are the interpolation of the analytical initial conditions. Once these are known, we reconstruct p using the compatibility conditions (22) with $\lambda = \frac{1}{2}$, which reads

$$p_h(x_\alpha, y_\beta) := \lambda \left(\int_{x_0}^{x_\alpha} S_u(\xi, y_\beta) d\xi + p_e(x_0, y_\beta) \right) + (1 - \lambda) \left(\int_{y_0}^{y_\beta} S_v(x_\alpha, \xi) d\xi + p_e(x_\alpha, y_0) \right), \quad (76b)$$

where, as everywhere else in this paper, the source terms are expanded on the finite element basis, and their integrals are simply evaluated by multiplication of the nodal array of source terms with the operators I_x and I_y . To solve the optimization problem (76a), we use the trust-region constrained method which is implemented in `scipy.optimize.minimize`. On the other hand, we recall that the so obtained p is not in both kernels of the two velocity evolution operators, but it carries an $O(h^M)$ error in the non-homogeneous case, because of the boundary conditions.

Finally, we will also use the simple strategy of running a long-time simulation and using its result as the equilibrium value for a perturbation simulation, adding the perturbation on top of it.

5 Stabilization methods in multi-dimensional Global Flux form

In this section, we adapt the SU and OSS stabilization techniques to the GF quadrature framework, including source terms as well. For both approaches, we will study the kernels, showing that Proposition 6 still holds, and verify the consistency estimates associated to Proposition 7.

5.1 SU-GF stabilization

We start from the integral form associated to the streamline upwind stabilization, presented in equation (51) and use the GF form (15). This leads to

$$\left\{ \begin{array}{l} \int_{\Omega} \alpha h \partial_x \varphi (\partial_t p_h + \partial_{xy} (G_p)_h) dx dy, \\ \int_{\Omega} \alpha h \partial_y \varphi (\partial_t p_h + \partial_{xy} (G_p)_h) dx dy, \\ \int_{\Omega} \alpha h \nabla \varphi \cdot \left[\partial_t \mathbf{v}_h + \nabla p_h - \begin{pmatrix} \partial_x (\mathcal{K}_u)_h \\ \partial_y (\mathcal{K}_v)_h \end{pmatrix} \right] dx dy. \end{array} \right. \quad (77)$$

Using the same approximation ansatz used for the GF Galerkin approximation, we can readily write the matrix form for the GF approximation:

$$\left\{ \begin{array}{l} \alpha h (D^x \otimes M_y \partial_t \mathbf{p} + D_x^x \otimes D_y (\mathbf{U} + \mathbf{V} - \mathbf{K}_p)), \\ \alpha h (M_x \otimes D^y \partial_t \mathbf{p} + D_x \otimes D_y^y (\mathbf{U} + \mathbf{V} - \mathbf{K}_p)), \\ \alpha h (D^x \otimes M_y \partial_t \mathbf{u} + D_x^x \otimes M_y (\mathbf{p} - \mathbf{K}_u)) + \\ \alpha h (M_x \otimes D^y \partial_t \mathbf{v} + M_x \otimes D_y^y (\mathbf{p} - \mathbf{K}_v)). \end{array} \right. \quad (78)$$

or, expanding the integrated velocities \mathbf{U} , and \mathbf{V} and sources $\mathbf{K}_u, \mathbf{K}_v, \mathbf{K}_p$

$$\left\{ \begin{array}{l} \text{ST}_{\text{SU-GF}}^u(\mathbf{u}, \mathbf{v}, \mathbf{p}) = \alpha h (D^x \otimes M_y \partial_t \mathbf{p} + D_x^x \otimes D_y (\mathbb{1}_x \otimes I_y \mathbf{u} + I_x \otimes \mathbb{1}_y \mathbf{v} - I_x \otimes I_y S_p)), \\ \text{ST}_{\text{SU-GF}}^v(\mathbf{u}, \mathbf{v}, \mathbf{p}) = \alpha h (M_x \otimes D^y \partial_t \mathbf{p} + D_x \otimes D_y^y (\mathbb{1}_x \otimes I_y \mathbf{u} + I_x \otimes \mathbb{1}_y \mathbf{v} - I_x \otimes I_y S_p)), \\ \text{ST}_{\text{SU-GF}}^p(\mathbf{u}, \mathbf{v}, \mathbf{p}) = \alpha h (D^x \otimes M_y \partial_t \mathbf{u} + D_x^x \otimes M_y (\mathbf{p} - I_x \otimes \mathbb{1}_y S_u)) + \\ \alpha h (M_x \otimes D^y \partial_t \mathbf{v} + M_x \otimes D_y^y (\mathbf{p} - \mathbb{1}_x \otimes I_y S_v)). \end{array} \right. \quad (79)$$

Comparing this expression to (52), one observes that the second derivatives are applied to the integrated, global quantities, which contain the sources and all the space derivatives, i.e., all terms governing the (discrete) steady states discussed in section 4. In contrast, standard approaches apply stabilization differently to different terms and thus equilibria between these terms are easily destroyed.

The full multi-dimensional GF Streamline Upwind stabilized scheme is defined by

$$\begin{aligned} R_c^u(u, v, p) + ST_{\text{SU-GF}}^u(u, v, p) &= 0, \\ R_c^v(u, v, p) + ST_{\text{SU-GF}}^v(u, v, p) &= 0, \\ R_c^p(u, v, p) + ST_{\text{SU-GF}}^p(u, v, p) &= 0, \end{aligned} \quad (80)$$

with GF Galerkin centered operators defined in (66b) and stabilization given by (79). The steady states of the stabilized scheme are characterized by the following statement.

Proposition 8 (Streamline Upwind stabilized GF scheme: discrete solutions and consistency). *The discrete steady kernel of the stabilized scheme (80) verifies both propositions 5 and 6.*

Proof. The proof of the first point is identical to those of propositions 5 and 6, applied to the discrete stabilization operators (78). \square

We recall that the consistency estimate is related to the fact that discrete solutions are obtained using a line-by-line/row-by-row projection (75). In particular, when this projection is performed with the LobattoIIIA solver, we obtain a consistency of order $K + 2$ for interpolation of degrees $K \geq 2$, see [29], which leads to the super-convergence result. We conclude that the SU-GF scheme has the same stationarity preservation properties as the unstabilized method.

5.2 OSS-GF stabilization

Similarly to the previous section, we now apply the variational form associated to the OSS stabilization method to the GF formulation:

$$\begin{cases} \int_{\Omega} \alpha h \partial_x \varphi (\partial_{xy}(G_p)_h - w^{\partial_{xy} G_p}) \, dx dy, \\ \int_{\Omega} \alpha h \partial_y \varphi (\partial_{xy}(G_p)_h - w^{\partial_{xy} G_p}) \, dx dy, \\ \int_{\Omega} \alpha h \partial_x \varphi [\partial_x(p - \mathcal{K}_u)_h - w^{\partial_x p}] \, dx dy + \int_{\Omega} \alpha h \partial_y \varphi [\partial_y(p - \mathcal{K}_v)_h - w^{\partial_y p}] \, dx dy, \end{cases} \quad (81)$$

complemented with the L^2 projections

$$\begin{cases} \int_{\Omega} \varphi (w^{\partial_{xy} G_p} - \partial_{xy}(G_p)_h) \, dx dy &= 0, \\ \int_{\Omega} \varphi (w^{\partial_x p} - \partial_x(p - \mathcal{K}_u)_h) \, dx dy &= 0, \\ \int_{\Omega} \varphi (w^{\partial_y p} - \partial_y(p - \mathcal{K}_v)_h) \, dx dy &= 0. \end{cases} \quad (82)$$

Differently from the standard formulation, in this case we do not have cancellation of so many terms in the assembly. However, all terms group together nicely in terms of the GF. After some simplifications, we obtain the following matrix form of the OSS-GF stabilization (cf. (65) and (58) for the notation):

$$\begin{cases} ST_{\text{OSS-GF}}^u(u, v, p) = \alpha h Z_x \otimes D_y (U + V - K_p), \\ ST_{\text{OSS-GF}}^v(u, v, p) = \alpha h D_x \otimes Z_y (U + V - K_p), \\ ST_{\text{OSS-GF}}^p(u, v, p) = \alpha h [Z_x \otimes M_y (p - K_u) + M_x \otimes Z_y (p - K_v)]. \end{cases} \quad (83)$$

These expressions are somewhat similar to (57), but involve now the multi-dimensional GFs, which is the key to the steady state preserving property of the method. The full expressions in terms of the arrays of pressure and velocities are easily obtained by combining the above formulas with (65). The full multi-dimensional GF OSS stabilized scheme is defined by

$$\begin{aligned} R_c^u(u, v, p) + ST_{\text{OSS-GF}}^u(u, v, p) &= 0, \\ R_c^v(u, v, p) + ST_{\text{OSS-GF}}^v(u, v, p) &= 0, \\ R_c^p(u, v, p) + ST_{\text{OSS-GF}}^p(u, v, p) &= 0, \end{aligned} \quad (84)$$

with GF Galerkin centered operators defined in (66b), and stabilization given by (83) combined with (65). The form of the OSS-GF stabilization allows to easily prove properties similar to those of the SU-GF scheme.

Proposition 9 (Orthogonal Subscale Stabilized GF scheme: discrete solutions and consistency). *The discrete steady kernel of the stabilized scheme (84) verifies both propositions 5 and 6.*

Proof. The proof of the first point is identical to those of propositions 5 and 6, applied to the discrete stabilization operators (83). \square

Once more we recall that the quality of the consistency estimate is related to the super-convergence of the LobattoIIIA ODE integrator [29] involved in the line-by-line/row-by-row projection (75). The analysis shows that the OSS-GF scheme has the same steady state preservation properties as the unstabilized method.

6 Explicit time integration using deferred correction

In all the previous formulations, we have always presented the time-continuous form. In order to obtain an explicit and arbitrarily high-order time discretization, we will employ the Deferred Correction (DeC) method [24, 43, 1, 40]. This technique consists of defining two discretizations: \mathcal{L}^2 a high order implicit method, e.g., Lobatto IIIA, and \mathcal{L}^1 an explicit low order version of \mathcal{L}^2 .

To define the high order operator \mathcal{L}^2 , we introduce a continuous FEM discretization of the time interval $[t_n, t_{n+1}]$ through some Lagrangian basis functions $\gamma_r(t)$ for $r = 0, \dots, M$, defined on the Gauss-Lobatto temporal sub-levels $t_n = t_n^0 < \dots < t_n^M = t_{n+1}$. For an ODE $q' + F(q) = 0$, let us denote by $q^m \approx q(t_n^m)$ for $m = 0, \dots, M$ the approximation of q in the sub-time level. Let \underline{q} denote the array of all the q^m . For each sub-level $m = 1, \dots, M$, we define the high-order operator

$$\mathcal{L}^{2,m}(\underline{q}) := q^m - q^0 + \sum_{r=0}^M F(q^r) \int_{t_n^0}^{t_n^m} \gamma_r(t) dt \approx q^m - q^0 + \int_{t_n^0}^{t_n^m} F(q(t)) dt. \quad (85)$$

We define $\vartheta_r^m := \frac{1}{\Delta t} \int_{t_n^0}^{t_n^m} \gamma_r(t) dt$. The equation $\mathcal{L}^2(\underline{q}) = 0$ is the Lobatto IIIA method with $M + 1$ stages. Instead of solving it directly, we introduce a low-order operator that will be actually solved, while the high-order operator will be used just as a correction term:

$$\mathcal{L}^{1,m}(\underline{q}) := q^m - q^0 + (t_n^m - t_n^0)F(q^0) \approx q^m - q^0 + \int_{t_n^0}^{t_n^m} F(q(t_n)) dt. \quad (86)$$

We define $\beta^m := \frac{t_n^m - t_n^0}{\Delta t}$. $\mathcal{L}^1(\underline{q}) = 0$ corresponds to a series of explicit Euler methods applied to different intervals. Moreover, in the \mathcal{L}^1 we can introduce further simplifications such as mass lumping or removing the stabilization, to create a very simple scheme to solve. The DeC iterative method is then defined by

$$\begin{cases} \underline{q}^{(0)} := (q(t_n), \dots, q(t_n)), \\ \mathcal{L}^1(\underline{q}^{(k)}) = \mathcal{L}^1(\underline{q}^{(k-1)}) - \mathcal{L}^2(\underline{q}^{(k-1)}), & k = 1, \dots, \kappa, \\ q_{n+1} := q^{(\kappa)}(t_n^M). \end{cases} \quad (87)$$

with κ the number of iterations performed. It can be shown that the order of accuracy of the method is the minimum between the order of accuracy of \mathcal{L}^2 and the number of iterations κ , under classical assumptions on the time-step size [1, 40]. Hence, it will be natural to consider \mathbb{P}^K spatial discretizations that lead to order $K + 1$ in the unsteady regime. Knowing that \mathcal{L}^2 achieves order $2M$ with Gauss-Lobatto points, we will set it such that $2M \geq K + 1$, so that at least order $K + 1$ is achieved in the \mathcal{L}^2 operator. Then, the number of iterations are naturally set to $\kappa := K + 1$ to have, for the whole DeC, a space-time order $K + 1$ at least.

The DeC allows to combine the spatial and time discretization into unique operators \mathcal{L}^1 and \mathcal{L}^2 . Let us therefore endow also the PDE variables with a superscript denoting the sub-time step stages of the

DeC. As an example, the SU \mathcal{L}^2 operator for the u equation reads

$$\begin{aligned} \mathcal{L}_u^{2,m}(q) := & (M_x \otimes M_y)(u^m - u^0) + \sum_{r=0}^M \vartheta_r^m \Delta t ((D_x \otimes M_y)p^r - (M_x \otimes M_y)S_u^r) \\ & + \alpha h (D^x \otimes M_y)(p^m - p^0) + \alpha h \sum_{r=0}^M \vartheta_r^m \Delta t ((D_x^x \otimes M_y)u^r + (D^x \otimes D_y)v^r - (D^x \otimes M_y)S_p^r), \end{aligned} \quad (88)$$

which, combined with the v and p equations create a coupled linear system of $3N_x N_y M$ equations. Since in our case M_x is diagonal (the quadrature rule used to compute the all matrices is given by the Gauss–Lobatto nodes that defining the Lagrangian basis function), this issue can be overcome by defining the \mathcal{L}^1 operator as

$$\mathcal{L}_u^{1,m}(q) := (M_x \otimes M_y)(u^m - u^0) + \beta_r^m \Delta t ((D_x \otimes M_y)p^0 - (M_x \otimes M_y)S_u^0), \quad (89)$$

which leads to an explicit scheme in the DeC formulation. This means that the complex SUPG structure of time derivative in the stabilization term can be simply solved within an explicit scheme. A detailed Fourier stability analysis of DeC time stepping with stabilized finite element discretizations, including both the SU and OSS stabilization methods, is provided in [41] for the one-dimensional advection equation. A two-dimensional extension on structured triangulations is presented in [42]. In this work, the time step is set to

$$\Delta t = \text{CFL} \frac{h}{c}.$$

Specific values of the CFL, and of other discretization parameters, are discussed in the next section. The GF version follows a similar approach, where we change the spatial discretization operators, i.e.,

$$\begin{aligned} \mathcal{L}_u^{2,m}(q) := & (M_x \otimes M_y)(u^m - u^0) + \sum_{r=0}^M \vartheta_r^m \Delta t ((D_x \otimes M_y)p^r - (D_x I_x \otimes M_y)S_u^r) \\ & + \alpha h (D^x \otimes M_y)(p^m - p^0) + \alpha h \sum_{r=0}^M \vartheta_r^m \Delta t (D_x^x \otimes D_y) ((1_x \otimes I_y)u^r + (I_y \otimes 1_y)v^r - (I_x \otimes I_y)S_p^r), \end{aligned} \quad (90)$$

to be consistent with the GF ones, as well as in the \mathcal{L}^1 operators.

For the sake of brevity, we do not expand in detail all the equations for the SUPG method, nor for the OSS methods, but similar arguments can be applied: stabilization terms are present only in the \mathcal{L}^2 operators where time derivative are replaced by $q^m - q^0$ for the m -th equation; all the GF operators are inserted both in \mathcal{L}^2 and \mathcal{L}^1 .

In the steady state regime, the time discretization plays no role. In particular, all terms vanish when the discrete data is in the kernel of the spatial discretization, so all the super-convergence results apply independently of the time scheme. More details can be found in [10].

7 Implementation and numerical validation

In this section, we validate the numerical method presented above with a series of tests with various source terms. We will start with Coriolis effects in Section 7.1, then we will add a mass source in Section 7.2, and in Section 7.3 we will end with the Stommel Gyre test that includes several sources at once. For each of them, we will perform different studies: steady state equilibrium study with convergence, characterization of the equilibrium and perturbation analysis.

Concerning the implementation, for all involved polynomials and quadrature rules, in space and time, we have used Gauss–Lobatto points that guarantee super-convergence in the steady state case. This choice, corresponding to the classical Spectral Element approach [46, 35], also makes the variational statement

Table 1: Vortex with Coriolis force: p and u errors and convergence rates with SU and OSS stabilization

		SU Q^1				SU-GF Q^1				OSS Q^1				OSS-GF Q^1			
N		err u	err p	O- u	O- p	err u	err p	O- u	O- p	err u	err p	O- u	O- p	err u	err p	O- u	O- p
20		7.9e-03	3.9e-03	0.0	0.0	2.5e-03	1.7e-03	0.0	0.0	6.0e-03	4.7e-03	0.0	0.0	2.6e-03	2.0e-03	3.1	2.3
40		1.6e-03	8.6e-04	2.3	2.2	6.4e-04	4.2e-04	2.0	2.0	1.3e-03	9.0e-04	2.2	2.4	6.5e-04	4.5e-04	2.0	2.2
80		3.4e-04	1.8e-04	2.2	2.3	1.6e-04	8.9e-05	2.0	2.2	3.2e-04	1.8e-04	2.1	2.3	1.6e-04	9.1e-05	2.0	2.3
160		8.0e-05	4.2e-05	2.1	2.1	3.9e-05	2.1e-05	2.0	2.1	7.8e-05	4.2e-05	2.0	2.1	3.9e-05	2.1e-05	2.0	2.1
320		2.0e-05	1.1e-05	2.0	2.0	9.8e-06	5.3e-06	2.0	2.0	2.0e-05	1.0e-05	2.0	2.0	9.8e-06	5.3e-06	2.0	2.0

		SU Q^2				SU-GF Q^2				OSS Q^2				OSS-GF Q^2			
N		err u	err p	O- u	O- p	err u	err p	O- u	O- p	err u	err p	O- u	O- p	err u	err p	O- u	O- p
10		1.1e-02	3.1e-03	0.0	0.0	7.6e-04	2.5e-04	0.0	0.0	9.0e-03	5.7e-03	0.0	0.0	8.2e-04	5.6e-04	4.3	4.5
20		2.9e-03	4.9e-04	2.0	2.7	1.3e-04	5.1e-05	2.5	2.3	2.2e-03	1.2e-03	2.1	2.2	1.4e-04	9.0e-05	2.5	2.6
40		7.8e-04	1.3e-04	1.9	1.9	8.2e-06	3.2e-06	4.0	4.0	6.2e-04	2.5e-04	1.8	2.3	8.7e-06	4.7e-06	4.0	4.3
80		1.7e-04	2.9e-05	2.2	2.2	5.1e-07	2.0e-07	4.0	4.0	1.8e-04	4.1e-05	1.8	2.6	5.3e-07	2.2e-07	4.0	4.4
160		3.2e-05	5.2e-06	2.4	2.5	3.1e-08	1.2e-08	4.0	4.0	4.8e-05	8.8e-06	1.9	2.2	3.2e-08	1.3e-08	4.0	4.1

		SU Q^3				SU-GF Q^3				OSS Q^3				OSS-GF Q^3			
N		err u	err p	O- u	O- p	err u	err p	O- u	O- p	err u	err p	O- u	O- p	err u	err p	O- u	O- p
6		1.1e-02	2.2e-03	0.0	0.0	1.4e-03	2.2e-04	0.0	0.0	1.4e-02	1.0e-02	0.0	0.0	1.4e-03	2.8e-04	0.2	2.0
13		1.6e-03	2.7e-04	2.5	2.7	4.6e-05	1.9e-05	4.4	3.2	2.5e-03	1.7e-03	2.2	2.3	4.7e-05	2.0e-05	4.4	3.4
26		8.3e-05	1.2e-05	4.3	4.5	2.0e-06	4.1e-07	4.6	5.5	3.8e-05	6.7e-06	6.0	8.0	2.0e-06	4.5e-07	4.6	5.5
53		4.3e-06	6.0e-07	4.2	4.2	5.6e-08	4.3e-09	5.0	6.4	1.8e-06	2.3e-07	4.3	4.7	5.6e-08	4.9e-09	5.0	6.3
106		2.6e-07	3.6e-08	4.0	4.0	1.7e-09	7.9e-11	5.0	5.7	1.0e-07	1.1e-08	4.1	4.5	1.7e-09	8.8e-11	5.0	5.8

		SU Q^4				SU-GF Q^4				OSS Q^4				OSS-GF Q^4			
N		err u	err p	O- u	O- p	err u	err p	O- u	O- p	err u	err p	O- u	O- p	err u	err p	O- u	O- p
5		2.0e-03	5.8e-04	0.0	0.0	1.6e-03	4.9e-04	0.0	0.0	2.8e-03	1.3e-03	0.0	0.0	1.6e-03	5.4e-04	2.9	2.6
10		5.4e-04	7.6e-05	1.9	2.9	9.5e-06	2.4e-06	7.4	7.7	2.9e-04	7.0e-05	3.3	4.2	9.5e-06	2.4e-06	7.4	7.8
20		2.3e-05	2.9e-06	4.6	4.7	4.2e-07	1.0e-07	4.5	4.5	1.4e-05	4.3e-06	4.3	4.0	4.2e-07	1.0e-07	4.5	4.5
40		1.2e-06	1.4e-07	4.3	4.4	6.6e-09	9.5e-10	6.0	6.7	1.2e-06	1.9e-07	3.6	4.5	6.6e-09	1.1e-09	6.0	6.6
80		4.9e-08	5.5e-09	4.6	4.6	1.1e-10	1.2e-11	6.0	6.4	8.6e-08	3.8e-08	3.7	2.3	1.1e-10	1.3e-11	6.0	6.4

		SU Q^5				SU-GF Q^5				OSS Q^5				OSS-GF Q^5			
N		err u	err p	O- u	O- p	err u	err p	O- u	O- p	err u	err p	O- u	O- p	err u	err p	O- u	O- p
4		5.1e-03	6.5e-04	0.0	0.0	9.2e-04	2.7e-04	0.0	0.0	6.1e-03	3.0e-03	0.0	0.0	9.2e-04	3.2e-04	2.8	3.1
8		2.0e-04	2.3e-05	4.6	4.8	1.2e-05	3.1e-06	6.3	6.4	3.0e-04	1.6e-04	4.3	4.3	1.2e-05	3.4e-06	6.3	6.5
16		6.2e-06	6.2e-07	5.1	5.2	1.2e-07	1.8e-08	6.6	7.4	6.4e-06	1.6e-06	5.6	6.6	1.2e-07	2.2e-08	6.6	7.3
32		1.1e-07	1.2e-08	5.8	5.7	9.0e-10	1.6e-10	7.1	6.8	5.8e-08	1.5e-08	6.8	6.8	9.1e-10	1.6e-10	7.1	7.1
64		1.7e-09	2.0e-10	6.0	5.9	2.1e-11	6.9e-12	5.4	4.5	6.5e-06	9.3e-06	-6.8	-9.3	2.1e-11	6.9e-12	5.4	4.6

in strong form (47) equivalent to the weak form, thanks to a discrete summation by parts property [35]. This also makes all the mass matrices diagonal.

In all the tests, we use CFL = 0.1 for all polynomial degrees smaller or equal to 5 and CFL = $\frac{1}{2(2p+1)}$ for higher degrees. For the SU stabilization, we will use $\alpha = 0.05$ for polynomial degrees less or equal to 5, and $\alpha = 0.02$ for higher degrees. For OSS, we will set $\alpha = 0.01$ for Q^1 and Q^2 , while $\alpha = 0.04$ for higher polynomials in all tests. These parameters turned out to be stable in all the performed simulations.

7.1 Steady equilibria with Coriolis force

We first study the approximation of steady equilibria for the system (23) with the Coriolis term only. In particular, let us consider the vortex solution (29)–(30) on the square $\Omega = [0, 1]^2$, with a Coriolis coefficient $c = 0.2$ and $P_0 = 1$. We choose $h(\rho) := 20e^{-100\rho^2}$ and thus $g(\rho) := \frac{1}{10}e^{-100\rho^2}$. For these choices the vortex perturbation $h(\rho)$ reaches values below machine precision at the boundaries. Hence, one can work with Neumann homogeneous boundary conditions on all variables.

We start by investigating the grid convergence of the schemes. To this end, we initialize the discrete solution with the analytical steady state interpolated at grid points, and we run until time $T = 1$. We then compute the errors with respect to the exact nodal solution. The computations have been run with both the SU and OSS stabilized schemes, in standard and GF formulation. Polynomial degrees $K \in \{1, \dots, 5\}$ are considered, with meshes of decreasing size as the degree is increased to avoid reaching machine accuracy already on the first meshes and to have comparable number of total degrees of freedom between different

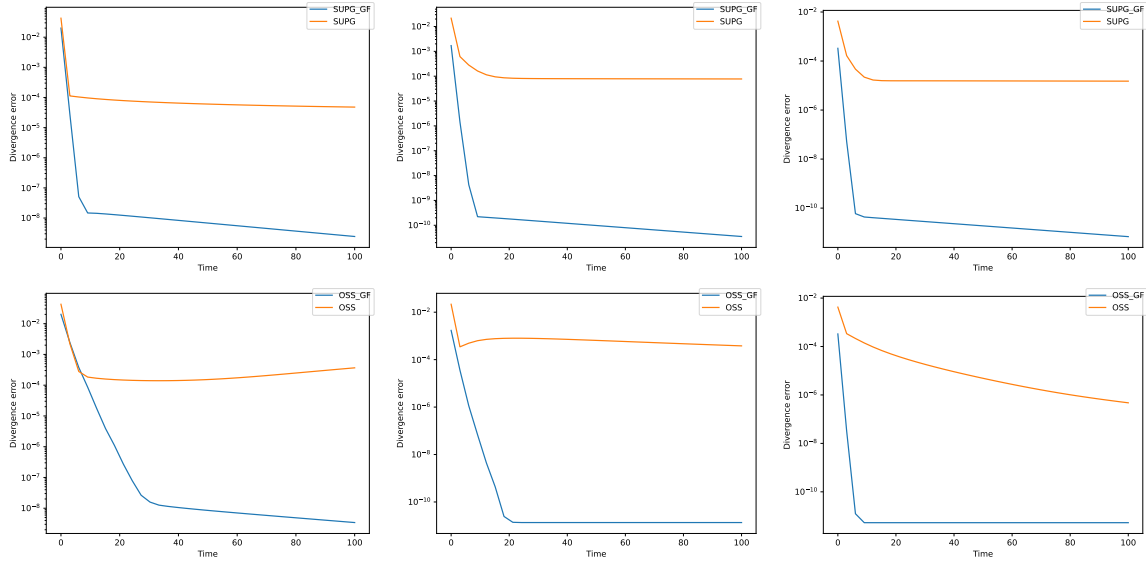


Figure 2: Vortex with Coriolis force: time evolution of the norm of discrete divergence ($D_x \otimes M_y u + M_x \otimes D_y v$ for classical methods and $D_x \otimes D_y I_y u + D_x I_x \otimes D_y v$ for GF simulations). Left column: Q^1 on 40×40 mesh. Middle column: Q^2 on 20×20 mesh. Right column: Q^3 with 13×13 mesh. Top: SU stabilization. Bottom: OSS stabilization.

orders. We report in Table 1 the resulting errors, and convergence rates. By symmetry, and to save space, only the u velocity component is reported.

The errors obtained with the GF formulations are systematically lower than those obtained with the standard scheme, even on the coarsest meshes. This initial error offset is variable and can go from a factor 2 to a full order of magnitude. As the meshes are refined, the results of both the SU stabilized method and the OSS confirm the theoretical $K + 2$ super-convergence estimates for $K \geq 2$. The error reductions observed when using the GF schemes are then between one and almost three orders of magnitude. The standard schemes require one or two additional mesh refinements to match the accuracy levels of the GF formulation.

We then consider long-time simulations to study the convergence to the discrete steady state. We measure the evolution of the discrete divergence operators relevant for each method: the usual Galerkin weak form $D_x \otimes M_y u + M_x \otimes D_y v$ for the standard schemes, and $D_x \otimes D_y I_y u + D_x I_x \otimes D_y v$ for the GF methods, as given in Propositions 5 and 6. The results are reported in Figure 2. The SU-GF converges extremely quickly (roughly 10 time steps), leading to values of the divergence well below the errors reported in Table 1 on the corresponding meshes. The standard SU scheme also seems to reach some stationary state, but the state is not in the kernel of the Galerkin weak form. We are unable to provide any characterization of this state, but it displays visible artefacts and a departure from circular symmetry, see Figure 3.

For the OSS stabilization the situation is very similar. Very low values of the discrete divergence are reached within few steps with the OSS-GF formulation, while the standard scheme does not seem to reach anything close to the kernel of the Galerkin divergence. We again are unable to characterize the long term solutions of the standard scheme in any way.

To give a qualitative feeling of the difference in performance between the GF formulation and the standard one, in Figure 3, we plot the velocity norm contours at time $T = 100$ for the standard scheme with SU stabilization and for the multi-dimensional GF scheme, as well as for the OSS stabilization. We compare the Q^1 results on the $N_x = N_y = 40$ mesh (the second mesh in the grid convergence), and the Q^3

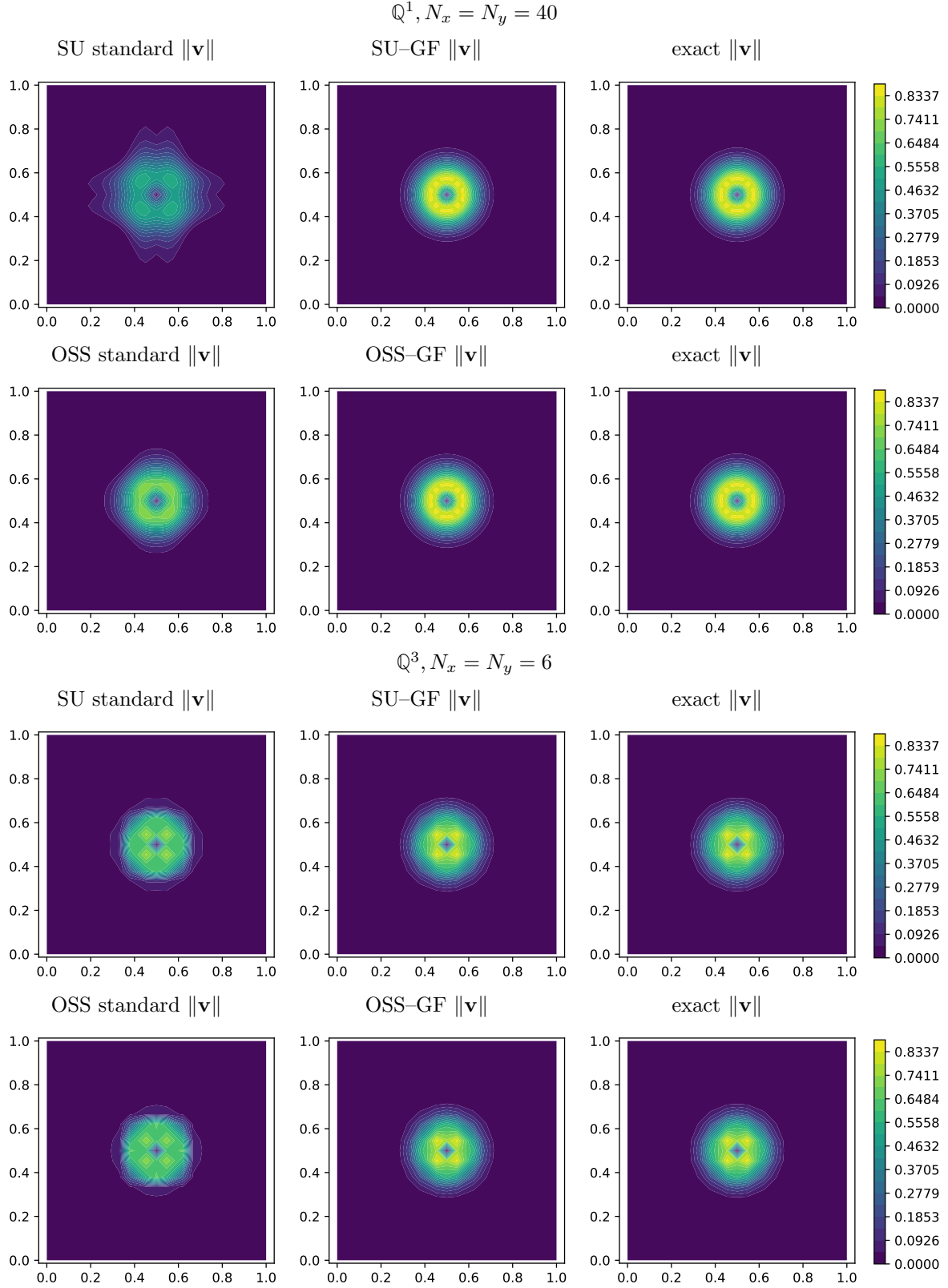


Figure 3: Vortex with Coriolis force: simulations at time $T = 100$ with \mathbb{Q}^1 elements and 40×40 cells (first and second row), and with \mathbb{Q}^3 with 6×6 cells (third and last row).

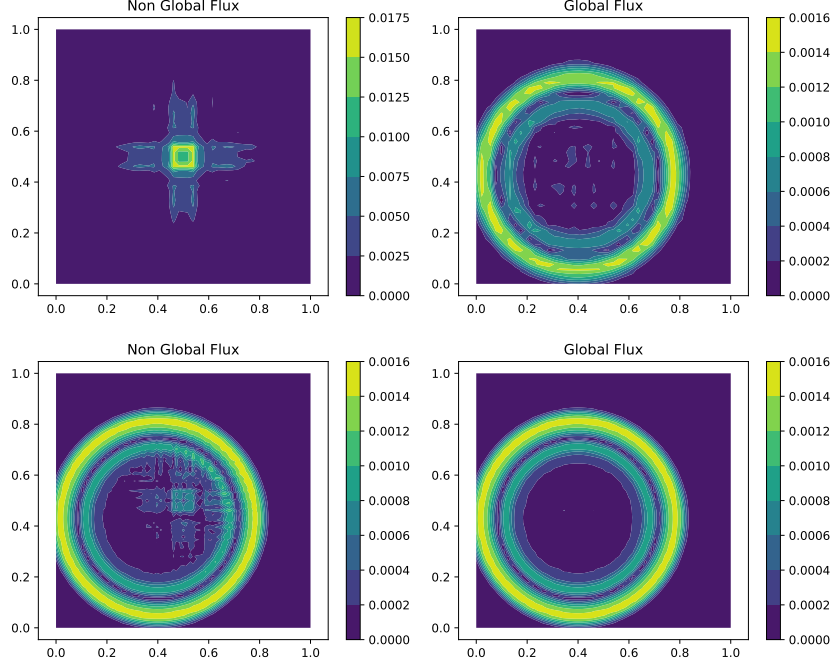


Figure 4: Vortex with Coriolis force: $\varepsilon = 10^{-2}$ perturbation of the optimal equilibrium solution. Plot of $\|\mathbf{u}_{eq} - \mathbf{u}_p^{\text{SU}}\|$, with \mathbf{u}_{eq} the optimized equilibrium (29). Top \mathbb{Q}^3 with 13 cells, bottom \mathbb{Q}^3 with 26 cells. All numerical results obtained using the SU method.

results on the coarsest mesh with $N_x = N_y = 6$ cells. In the rightmost figure, we report for comparison the exact solution. Clearly, even on these coarse meshes, the results of the GF methods are almost indistinguishable from the exact ones. The standard schemes break the structure of the solution and dissipate it. The longer the final time, the stronger the effect of this dissipation.

Finally, we perform a perturbation analysis, which is classical in the study of stationarity preserving discretizations: The main reason for developing a stationarity preserving method is not to preserve just the steady state, but to ensure that physical perturbations of a steady state are not disturbed by spurious numerical perturbations originating from the steady state itself. We perform this test on the vortex solution. We use the optimization process described in section 4.2.3 to get discrete well-prepared initial conditions, and then add a local perturbation to the pressure of the form

$$\delta_p(x) = \varepsilon e^{-\frac{1}{2(1-\rho(x)/r_0)^2} + \frac{1}{2}}, \quad (91)$$

where $\mathbf{x}_p = (0.4, 0.43)$, and $\rho(x) = \|\mathbf{x} - \mathbf{x}_p\|$, with $r_0 = 0.1$.

Starting from this perturbed state, we evolve the solution until time $T = 0.35$. We only discuss the results obtained with the SU methods, since those with OSS are very similar. In Figure 4, we test the perturbation with $\varepsilon = 10^{-2}$, applied on top of the optimization-based well-prepared equilibrium solution for various schemes. We observe that SU-GF is able to accurately describe the motion of the perturbation with no spurious effects even on a very coarse 13×13 mesh. The standard SU scheme on this mesh does not allow even to see the perturbation. Of course, mesh refinement reduces spurious artefacts and we can see a better result on a 26×26 discretization of the domain.

We then repeat the test with $\varepsilon = 10^{-6}$. The results are reported on Figure 5. The SU-GF method allows again to obtain an excellent resolution already on the coarse 13×13 mesh. For the standard method, in this case refining the mesh to 26×26 is not sufficient to capture such a small feature. Note that these results are obtained with quadratic and cubic polynomial degrees. This shows the advantage

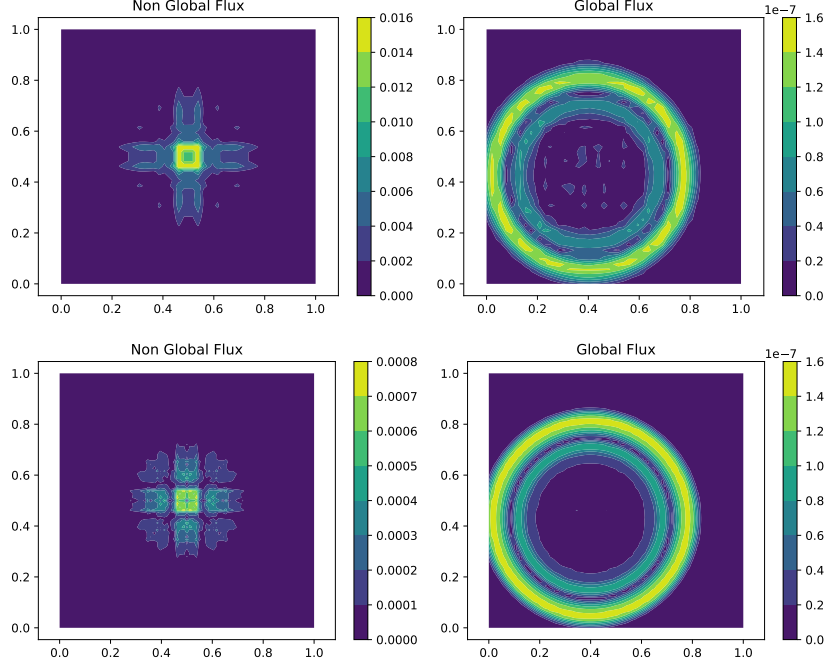


Figure 5: Vortex with Coriolis force: $\varepsilon = 10^{-6}$ perturbation of the optimal equilibrium solution. Plot of $\|\mathbf{u}_{eq} - \mathbf{u}_p^{\text{SU}}\|$, with \mathbf{u}_{eq} the optimized equilibrium (29). Top \mathbb{Q}^3 with 13 cells, bottom \mathbb{Q}^3 with 26 cells. All numerical results obtained using the SU method.

of combining high-order schemes and stationarity preservation. As one may expect, for very small values of the perturbation, the quality of the results still shows some dependence on the mesh size, and on the initialization strategy. However, the GF methods show systematically superior results.

7.2 Mass source cases

We now study the case involving a mass source as introduced in Section 2.2. This is a very interesting case where the truly multi-dimensional nature of the GF formulation is necessary to balance the divergence with the source. We consider both the steady solution (33) and the time dependent solution (34) as this allows to show the performance outside equilibrium.

7.2.1 Translating solution

We start from computing the convergence to the translating solution (34) to check that the GF methods maintain the classical order of accuracy in the non-stationary regime. We consider the particular case of (34) with $h(x, y, t) \equiv 0$, with $p_0 = 1$, $b = 0.001$, $\mathbf{a} = (-0.1, 0.1)$, $g(x, y) = e^{-100((x-x_0)^2 + (y-y_0)^2)}$, $x_0 = 0.65$, $y_0 = 0.39$. The final time of the simulation is set to $T = 0.1$. We compute the solutions with the SU and OSS stabilization methods, using both the GF and standard formulations.

The results for polynomial degrees K from 1 to 4 are reported in Table 2. To save space, only the u velocity component is reported. The convergence orders are in between $K + \frac{1}{2}$ and $K + 1$ for the GF schemes, and in between K and $K + \frac{1}{2}$ for the standard one. These confirm reasonably the expected $K + 1$ accuracy of the methods. Even if it is not a steady case, GF schemes seem to perform a little better, with errors systematically below those of the standard method.

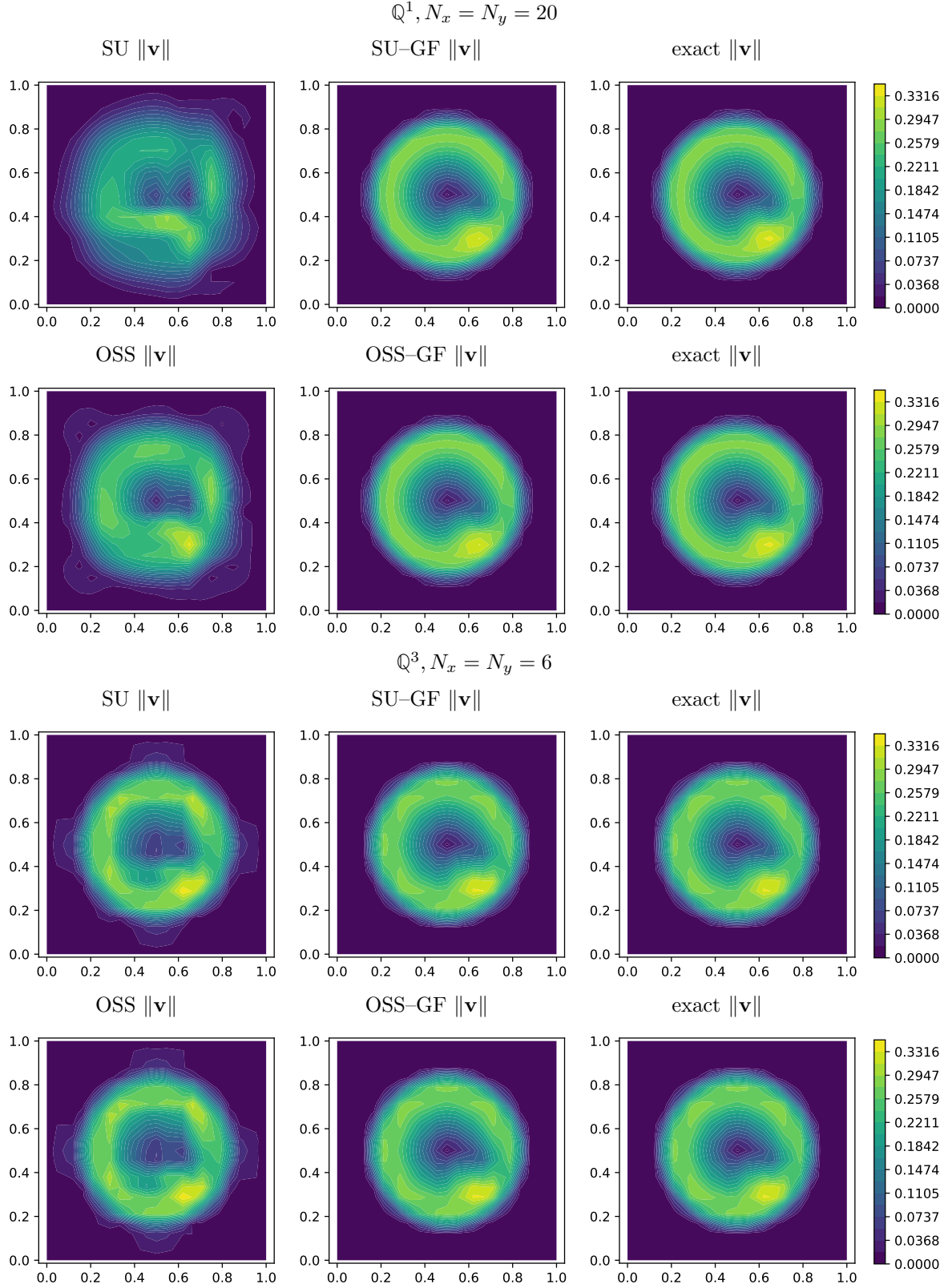


Figure 6: Vortex with mass source term: simulations at time $T = 100$ with \mathbb{Q}^1 elements and 40×40 cells (top) and with \mathbb{Q}^3 with 6×6 cells

Table 2: Translating solution with mass source: p and u errors and convergence rates with SU and OSS stabilization

SU Q^1					SU-GF Q^1					OSS Q^1					OSS-GF Q^1				
N	err u	err p	O- u	O- p	err u	err p	O- u	O- p	err u	err p	O- u	O- p	err u	err p	O- u	O- p			
10	2.1e-04	9.1e-04	0.0	0.0	8.0e-05	1.6e-04	0.0	0.0	2.3e-04	9.5e-04	0.0	0.0	6.5e-05	1.7e-04	0.0	0.0			
20	1.3e-04	2.5e-04	0.8	1.9	5.5e-05	8.7e-05	0.5	0.9	1.4e-04	2.4e-04	0.7	2.0	5.4e-05	9.0e-05	0.3	0.9			
40	4.1e-05	5.4e-05	1.6	2.2	2.0e-05	2.4e-05	1.5	1.9	4.3e-05	5.3e-05	1.7	2.2	2.0e-05	2.4e-05	1.5	1.9			
80	1.1e-05	1.3e-05	1.9	2.1	5.2e-06	5.9e-06	1.9	2.0	1.1e-05	1.3e-05	2.0	2.1	5.2e-06	5.9e-06	1.9	2.0			
160	2.7e-06	3.2e-06	2.0	2.0	1.3e-06	1.5e-06	2.0	2.0	2.8e-06	3.1e-06	2.0	2.0	1.3e-06	1.5e-06	2.0	2.0			

SU Q^2					SU-GF Q^2					OSS Q^2					OSS-GF Q^2				
N	err u	err p	O- u	O- p	err u	err p	O- u	O- p	err u	err p	O- u	O- p	err u	err p	O- u	O- p			
5	2.7e-04	7.0e-04	0.0	0.0	2.4e-04	4.9e-04	0.0	0.0	2.7e-04	7.7e-04	0.0	0.0	2.0e-04	5.2e-04	0.0	0.0			
10	1.8e-04	1.6e-04	0.6	2.1	4.0e-05	6.9e-05	2.6	2.8	2.1e-04	1.5e-04	0.3	2.3	4.0e-05	7.3e-05	2.3	2.8			
20	3.1e-05	2.9e-05	2.6	2.5	5.3e-06	6.0e-06	2.9	3.5	4.3e-05	3.4e-05	2.3	2.2	5.9e-06	8.2e-06	2.8	3.2			
40	5.1e-06	6.7e-06	2.6	2.1	6.8e-07	7.4e-07	2.9	3.0	9.5e-06	7.2e-06	2.2	2.2	9.0e-07	1.5e-06	2.7	2.4			
80	7.1e-07	1.3e-06	2.8	2.3	1.1e-07	8.3e-08	2.6	3.1	2.0e-06	1.7e-06	2.3	2.1	1.9e-07	3.0e-07	2.3	2.3			

SU Q^3					SU-GF Q^3					OSS Q^3					OSS-GF Q^3				
N	err u	err p	O- u	O- p	err u	err p	O- u	O- p	err u	err p	O- u	O- p	err u	err p	O- u	O- p			
3	2.9e-04	8.0e-04	0.0	0.0	2.8e-04	6.4e-04	0.0	0.0	2.9e-04	8.5e-04	0.0	0.0	2.5e-04	6.6e-04	0.0	0.0			
6	1.7e-04	2.2e-04	0.7	1.8	6.9e-05	6.8e-05	2.0	3.2	1.9e-04	2.5e-04	0.6	1.7	6.9e-05	7.2e-05	1.9	3.2			
13	9.5e-06	1.7e-05	3.7	3.3	2.7e-06	1.9e-06	4.2	4.6	1.0e-05	2.0e-05	3.8	3.3	2.7e-06	2.0e-06	4.2	4.6			
26	6.6e-07	6.0e-07	3.9	4.8	9.3e-08	1.1e-07	4.8	4.2	7.7e-07	6.5e-07	3.7	4.9	9.5e-08	1.2e-07	4.8	4.1			
53	3.8e-08	2.4e-08	4.0	4.5	5.6e-09	6.5e-09	3.9	3.9	4.4e-08	2.5e-08	4.0	4.6	5.5e-09	7.3e-09	4.0	4.0			

SU Q^4					SU-GF Q^4					OSS Q^4					OSS-GF Q^4				
N	err u	err p	O- u	O- p	err u	err p	O- u	O- p	err u	err p	O- u	O- p	err u	err p	O- u	O- p			
2	6.7e-04	9.8e-04	0.0	0.0	5.7e-04	7.8e-04	0.0	0.0	6.7e-04	1.0e-03	0.0	0.0	5.4e-04	8.1e-04	0.0	0.0			
5	7.3e-05	9.9e-05	2.4	2.5	4.7e-05	3.4e-05	2.7	3.4	6.8e-05	1.2e-04	2.5	2.4	4.7e-05	3.5e-05	2.7	3.4			
10	3.8e-06	3.5e-06	4.3	4.8	7.5e-07	7.4e-07	6.0	5.5	5.2e-06	4.2e-06	3.7	4.8	7.9e-07	8.9e-07	5.9	5.3			
20	1.2e-07	1.5e-07	4.9	4.6	2.2e-08	1.8e-08	5.1	5.3	1.5e-07	1.9e-07	5.1	4.5	2.3e-08	2.3e-08	5.1	5.3			
40	5.9e-09	7.2e-09	4.4	4.4	3.9e-09	2.7e-09	2.5	2.7	6.0e-09	9.0e-09	4.7	4.4	3.9e-09	2.7e-09	2.6	3.1			

7.2.2 Steady solution

We now consider (33) with h, g defined by $h(\rho) = 20e^{-100\rho^2}$, with ρ the distance from the center of the domain, and $g(x, y) := \frac{1}{100}e^{-100\rho_1^2}$, where $\rho_1 := \|\mathbf{x} - \mathbf{x}_1\|$, with $\mathbf{x}_1 = (0.65, 0.39)^T$. This solution defines a steady vortex with a scalar (mass/pressure) source added in \mathbf{x}_1 . We start by considering the solutions at time $T = 100$ to see the qualitative improvement brought by the GF approach. As before, we plot the norm of the velocity, for both the SU and OSS stabilized methods in both standard and GF formulation. Figure 6 reports the contour plots for the Q^1 case on the coarse $N_x = N_y = 20$ mesh, and for the Q^3 case on the $N_x = N_y = 6$ one. As before, already on these coarse meshes, the GF results are indistinguishable from the exact solution. The standard schemes break the circular symmetric structure of the solution, due to mismatch between the Galerkin term and the numerical dissipation, which precludes the stationarity preservation property.

Next, we consider a study of grid convergence. As before, we initialize the solution by sampling the exact one at nodes, and then run the schemes until a final time $T = 1$. Tables 3 reports the errors and the convergence rates for the SU and OSS stabilization methods, for polynomial degrees from 1 to 5. The error is measured in this case by comparing, at final time, the value of the nodal approximation of the steady state residual. To save space, only the u velocity component is reported. We can see that the theoretical $K + 2$ super-convergence for the GF method is confirmed also for this case. As for the other cases, the GF formulation gives systematically lower errors, starting with the coarsest meshes where the errors are about half. As the mesh is refined, this error gain goes up to a factor 10 or 50 due to the super-convergence of the GF schemes.

For the GF case, we report on figure 7 the norm of $D_x \otimes D_y I_y u + D_x I_x \otimes D_y v - D_x I_x \otimes D_y I_y S_p$, while for the standard case we plot the norm of $D_x \otimes M_y u + M_x \otimes D_y v - M_x \otimes M_y S_p$. Boundaries are excluded in both computations. We can observe that the standard residual converges with order K at most, while the GF converges with order $K + 1$ for all $K \geq 2$, as a consequence of its super-convergence properties.

Table 3: Vortex with mass source: p and u errors and convergence rates with SU and OSS stabilization

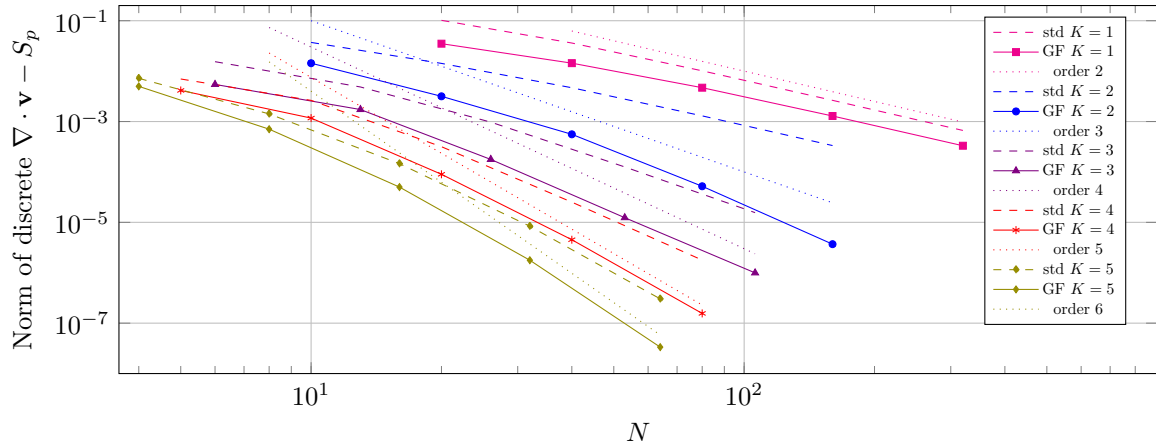
N	SU Q^1				SU-GF Q^1				OSS Q^1				OSS-GF Q^1			
	err u	err p	O- u	O- p	err u	err p	O- u	O- p	err u	err p	O- u	O- p	err u	err p	O- u	O- p
20	5.0e-03	2.3e-03	0.0	0.0	1.9e-03	9.5e-04	0.0	0.0	4.2e-03	3.2e-03	0.0	0.0	2.1e-03	1.3e-03	0.0	0.0
40	1.3e-03	5.5e-04	1.9	2.1	4.1e-04	2.5e-04	2.2	1.9	9.6e-04	6.9e-04	2.1	2.2	4.5e-04	3.1e-04	2.2	2.0
80	2.8e-04	1.3e-04	2.2	2.1	9.9e-05	6.3e-05	2.1	2.0	2.1e-04	1.5e-04	2.2	2.2	1.0e-04	7.2e-05	2.1	2.1
160	5.8e-05	3.2e-05	2.3	2.0	2.5e-05	1.6e-05	2.0	2.0	5.1e-05	3.4e-05	2.1	2.1	2.5e-05	1.7e-05	2.0	2.1
320	1.3e-05	7.7e-06	2.2	2.0	6.2e-06	3.8e-06	2.0	2.0	1.2e-05	8.1e-06	2.0	2.1	6.2e-06	4.0e-06	2.0	2.1

N	SU Q^2				SU-GF Q^2				OSS Q^2				OSS-GF Q^2			
	err u	err p	O- u	O- p	err u	err p	O- u	O- p	err u	err p	O- u	O- p	err u	err p	O- u	O- p
10	4.9e-03	1.5e-03	0.0	0.0	1.9e-03	9.0e-04	0.0	0.0	4.3e-03	2.5e-03	0.0	0.0	2.1e-03	1.4e-03	0.0	0.0
20	1.6e-03	3.1e-04	1.6	2.3	2.2e-04	8.6e-05	3.2	3.4	1.1e-03	4.4e-04	2.0	2.5	2.4e-04	1.4e-04	3.1	3.4
40	4.4e-04	7.4e-05	1.8	2.1	1.8e-05	6.1e-06	3.6	3.8	3.0e-04	7.1e-05	1.8	2.6	1.9e-05	9.1e-06	3.7	3.9
80	1.1e-04	1.7e-05	2.0	2.2	1.2e-06	4.6e-07	3.9	3.7	9.2e-05	1.7e-05	1.7	2.1	1.2e-06	5.3e-07	4.0	4.1
160	2.4e-05	3.1e-06	2.2	2.4	7.2e-08	3.3e-08	4.0	3.8	2.6e-05	4.7e-06	1.8	1.8	7.4e-08	3.4e-08	4.0	4.0

N	SU Q^3				SU-GF Q^3				OSS Q^3				OSS-GF Q^3			
	err u	err p	O- u	O- p	err u	err p	O- u	O- p	err u	err p	O- u	O- p	err u	err p	O- u	O- p
6	5.5e-03	1.7e-03	0.0	0.0	1.8e-03	6.4e-04	0.0	0.0	5.4e-03	2.0e-03	0.0	0.0	1.8e-03	7.0e-04	0.0	0.0
13	1.1e-03	2.0e-04	2.0	2.8	1.9e-04	6.1e-05	2.9	3.0	1.1e-03	2.4e-04	2.0	2.7	1.9e-04	6.5e-05	2.9	3.1
26	1.8e-04	1.5e-05	2.6	3.8	1.1e-05	3.5e-06	4.1	4.1	1.8e-04	1.7e-05	2.6	3.8	1.1e-05	3.7e-06	4.1	4.2
53	1.7e-05	1.1e-06	3.4	3.7	4.1e-07	1.1e-07	4.7	4.9	1.6e-05	1.2e-06	3.4	3.8	4.1e-07	1.1e-07	4.7	4.9
106	1.3e-06	6.7e-08	3.7	4.0	1.3e-08	1.9e-09	4.9	5.9	1.2e-06	6.8e-08	3.8	4.1	1.4e-08	3.2e-09	4.9	5.2

N	SU Q^4				SU-GF Q^4				OSS Q^4				OSS-GF Q^4			
	err u	err p	O- u	O- p	err u	err p	O- u	O- p	err u	err p	O- u	O- p	err u	err p	O- u	O- p
5	4.2e-03	1.0e-03	0.0	0.0	1.6e-03	5.8e-04	0.0	0.0	4.0e-03	1.3e-03	0.0	0.0	1.6e-03	6.7e-04	0.0	0.0
10	8.8e-04	9.1e-05	2.2	3.5	1.9e-04	5.3e-05	3.1	3.5	8.8e-04	1.1e-04	2.2	3.6	2.0e-04	5.8e-05	3.1	3.5
20	8.9e-05	6.9e-06	3.3	3.7	7.6e-06	1.8e-06	4.7	4.9	8.8e-05	8.7e-06	3.3	3.6	7.6e-06	1.9e-06	4.7	4.9
40	5.5e-06	2.7e-07	4.0	4.7	1.9e-07	3.8e-08	5.4	5.6	5.4e-06	3.4e-07	4.0	4.7	1.9e-07	3.9e-08	5.4	5.6
80	3.3e-07	1.5e-08	4.0	4.2	3.3e-09	6.7e-10	5.8	5.8	3.3e-07	2.0e-08	4.0	4.1	5.4e-09	3.1e-09	5.1	3.7

N	SU Q^5				SU-GF Q^5				OSS Q^5				OSS-GF Q^5			
	err u	err p	O- u	O- p	err u	err p	O- u	O- p	err u	err p	O- u	O- p	err u	err p	O- u	O- p
4	4.0e-03	1.1e-03	0.0	0.0	2.0e-03	8.2e-04	0.0	0.0	3.9e-03	1.4e-03	0.0	0.0	2.0e-03	9.5e-04	0.0	0.0
8	6.6e-04	5.7e-05	2.6	4.3	1.5e-04	3.2e-05	3.8	4.7	6.4e-04	7.5e-05	2.6	4.2	1.5e-04	3.6e-05	3.8	4.7
16	5.3e-05	2.8e-06	3.6	4.3	6.2e-06	1.3e-06	4.5	4.6	5.3e-05	3.9e-06	3.6	4.3	6.2e-06	1.4e-06	4.5	4.7
32	2.9e-06	1.2e-07	4.2	4.5	1.1e-07	2.2e-08	5.8	5.9	2.7e-06	1.8e-07	4.3	4.4	1.1e-07	2.3e-08	5.8	5.9
64	8.5e-08	2.5e-09	5.1	5.6	1.1e-09	1.1e-10	6.6	7.6	8.0e-08	5.3e-09	5.1	5.1	5.1e-09	3.4e-09	4.4	2.8


 Figure 7: Steady vortex with mass source: convergence with respect to the number of elements in x of L^2 norm of $\nabla \cdot \mathbf{v} - S_p$ of the analytical solution discretized in standard (std) way or with the GF technique.

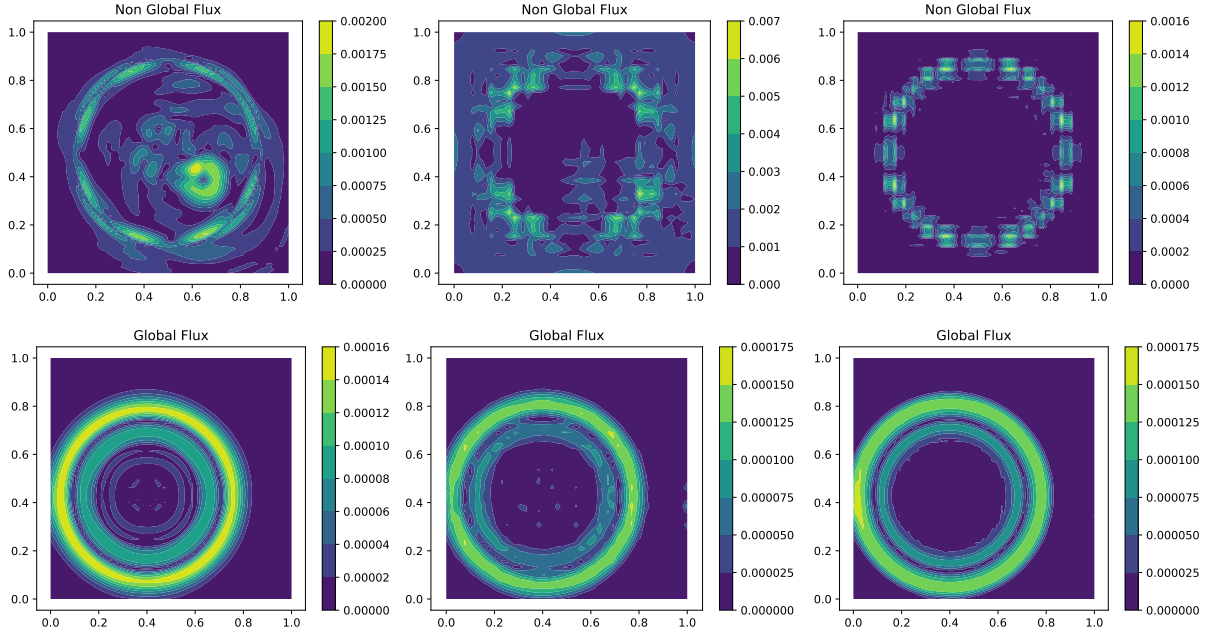


Figure 8: Vortex with mass source term: $\epsilon = 10^{-3}$ pressure perturbation of the optimal equilibrium solution, see Section 4.2.3. Plot of the $\|\mathbf{v}_{eq} - \mathbf{v}_p^{OSS}\|$, with \mathbf{v}_{eq} the equilibrium velocity. Left Q^1 with 80×80 cells, center Q^3 with 13 cells, right Q^3 with 26 cells. Numerical solutions obtained with the OSS (top) and OSS-GF (bottom) methods.

Finally, we consider the evolution of a small perturbation of the steady state. Equilibrium initial data is prepared using the optimization process of Section 4.2.3. A pressure perturbation of the form (91) with $\varepsilon = 10^{-3}$ is then added. In this case, we report in Figure 8 the results of the OSS method; the ones obtained with the SU schemes are very similar. The plots show the OSS solutions for $K = 1$ on a relatively fine 80×80 mesh, and for $K = 3$ on coarse 13×13 and 26×26 meshes. The OSS-GF method shows huge superiority with respect to the standard formulation both in the high and in the low order case. In the standard case, in particular, we can clearly see that the source term is perturbing the solution in the right bottom quadrant of the domain, while other errors spread around the exact solution profile. In this case, even refining the mesh to $N_x = N_y = 26$ does not allow to capture the perturbation with the standard scheme.

7.3 Stommel Gyre test case

We now consider the Stommel Gyre test case described in Section 2.3. This problem involves several sources of different forms. The contours of the exact velocity and pressure are reported for completeness in Figure 9. The precise test description is provided in Section 2.3. In the simulations, we have set the solution parameters to $\lambda = b = 1$ (domain), $c_1 = c_0 = f = 0.01$ (friction), $F = 0.1$ (wind force). Note that this is a non-compact case, for which the Dirichlet conditions allow a reasonable prediction already with the non-stationary preserving methods.

We start by studying the error with respect to exact solution for various mesh sizes. As done in the previous cases, we start from the exact nodal values, and run simulations until the final time $T = 1$. Table 4 shows the errors and convergence orders obtained with the SU stabilized schemes with polynomial degrees K from 1 to 5. Once again, we observe the super-convergence predicted by the analysis of Section 4.2.2, with dramatic error reductions for $K \geq 3$. The super-convergence is also visualized on Figure 10 in terms of convergence of the divergence operator. As before, we compute the norm of $D_x \otimes D_y I_y \mathbf{u} + D_x I_x \otimes D_y \mathbf{v}$ for the GF method, and of $D_x \otimes M_y \mathbf{u} + M_x \otimes D_y \mathbf{v}$ for the standard case. Domain boundaries are ex-

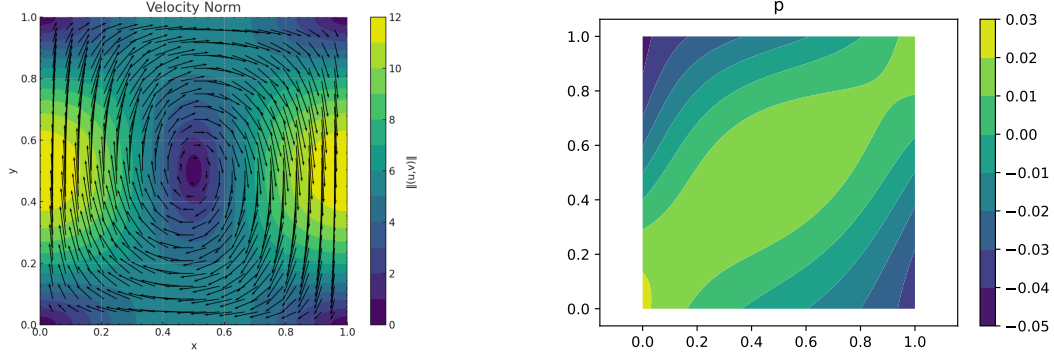


Figure 9: Stommel Gyre solution for $\lambda = b = 1$, $f_0 = \varphi_0 = R = 0.01$, $F = 0.1$, left velocity norm contour and velocity vector field, right pressure contour levels

Table 4: Stommel Gyre test convergence results with SU stabilization for u , v and p

SU Q^1							SU-GF Q^1						
N	err u	err v	err p	ord u	ord v	ord p	N	err u	err v	err p	ord u	ord v	ord p
20	8.51e-03	8.99e-03	5.49e-03	0.00	0.00	0.00	20	5.62e-03	5.93e-03	3.15e-03	0.00	0.00	0.00
40	2.21e-03	2.32e-03	1.32e-03	1.94	1.95	2.06	40	1.37e-03	1.43e-03	7.12e-04	2.03	2.05	2.15
80	5.63e-04	5.89e-04	3.20e-04	1.98	1.98	2.04	80	3.28e-04	3.41e-04	1.66e-04	2.07	2.07	2.10
160	1.42e-04	1.48e-04	7.90e-05	1.99	1.99	2.02	160	7.87e-05	8.16e-05	4.01e-05	2.06	2.06	2.05
320	3.56e-05	3.71e-05	1.96e-05	1.99	2.00	2.01	320	1.90e-05	1.97e-05	9.86e-06	2.05	2.05	2.03

SU Q^2							SU-GF Q^2						
N	err u	err v	err p	ord u	ord v	ord p	N	err u	err v	err p	ord u	ord v	ord p
10	4.88e-03	5.07e-03	3.05e-03	0.00	0.00	0.00	10	6.18e-05	4.62e-05	2.10e-05	0.00	0.00	0.00
20	8.76e-04	9.00e-04	5.89e-04	2.48	2.49	2.37	20	4.42e-06	3.02e-06	1.41e-06	3.81	3.94	3.90
40	1.38e-04	1.41e-04	9.73e-05	2.67	2.67	2.60	40	2.97e-07	1.95e-07	9.42e-08	3.90	3.95	3.90
80	1.97e-05	2.01e-05	1.43e-05	2.80	2.82	2.77	80	1.92e-08	1.24e-08	6.18e-09	3.95	3.98	3.93
160	2.69e-06	2.68e-06	1.95e-06	2.87	2.90	2.87	160	1.22e-09	7.81e-10	3.98e-10	3.98	3.99	3.96

SU Q^3							SU-GF Q^3						
N	err u	err v	err p	ord u	ord v	ord p	N	err u	err v	err p	ord u	ord v	ord p
6	3.01e-04	3.26e-04	1.84e-04	0.00	0.00	0.00	6	1.21e-05	8.29e-06	3.68e-06	0.00	0.00	0.00
13	1.64e-05	1.55e-05	9.02e-06	3.76	3.94	3.90	13	2.67e-07	1.74e-07	6.02e-08	4.94	5.00	5.32
26	1.10e-06	9.70e-07	5.69e-07	3.90	4.00	3.99	26	8.28e-09	5.32e-09	1.27e-09	5.01	5.03	5.57
53	6.59e-08	5.59e-08	3.36e-08	3.95	4.01	3.97	53	2.33e-10	1.49e-10	2.04e-11	5.01	5.02	5.80
106	4.17e-09	3.46e-09	2.10e-09	3.98	4.01	4.00	106	7.20e-12	4.57e-12	4.27e-13	5.02	5.02	5.58

SU Q^4							SU-GF Q^4						
N	err u	err v	err p	ord u	ord v	ord p	N	err u	err v	err p	ord u	ord v	ord p
5	2.34e-05	3.13e-05	1.46e-05	0.00	0.00	0.00	5	8.22e-07	4.37e-07	2.28e-07	0.00	0.00	0.00
10	1.04e-06	1.28e-06	6.23e-07	4.49	4.61	4.55	10	1.37e-08	6.95e-09	3.14e-09	5.91	5.98	6.18
20	3.98e-08	4.63e-08	2.31e-08	4.71	4.79	4.76	20	2.17e-10	1.08e-10	3.48e-11	5.98	6.01	6.50
40	1.40e-09	1.57e-09	7.89e-10	4.83	4.88	4.87	40	3.38e-12	1.67e-12	3.47e-13	6.01	6.02	6.65
80	4.72e-11	5.10e-11	2.58e-11	4.89	4.94	4.93	80	7.65e-14	5.76e-14	3.08e-15	5.46	4.86	6.82

SU Q^5							SU-GF Q^5						
N	err u	err v	err p	ord u	ord v	ord p	N	err u	err v	err p	ord u	ord v	ord p
4	1.88e-06	2.98e-06	1.31e-06	0.00	0.00	0.00	4	8.65e-08	4.78e-08	1.99e-08	0.00	0.00	0.00
8	3.49e-08	5.01e-08	2.39e-08	5.75	5.90	5.77	8	7.10e-10	3.55e-10	1.57e-10	6.93	7.07	6.99
16	6.06e-10	8.08e-10	4.02e-10	5.85	5.95	5.89	16	5.59e-12	2.65e-12	9.74e-13	6.99	7.07	7.33
32	9.97e-12	1.27e-11	6.51e-12	5.92	5.99	5.95	32	5.52e-14	3.91e-14	6.50e-15	6.66	6.08	7.23
64	1.55e-13	2.15e-13	1.04e-13	6.01	5.89	5.97	64	6.41e-14	6.33e-14	3.29e-15	-0.22	-0.69	0.98

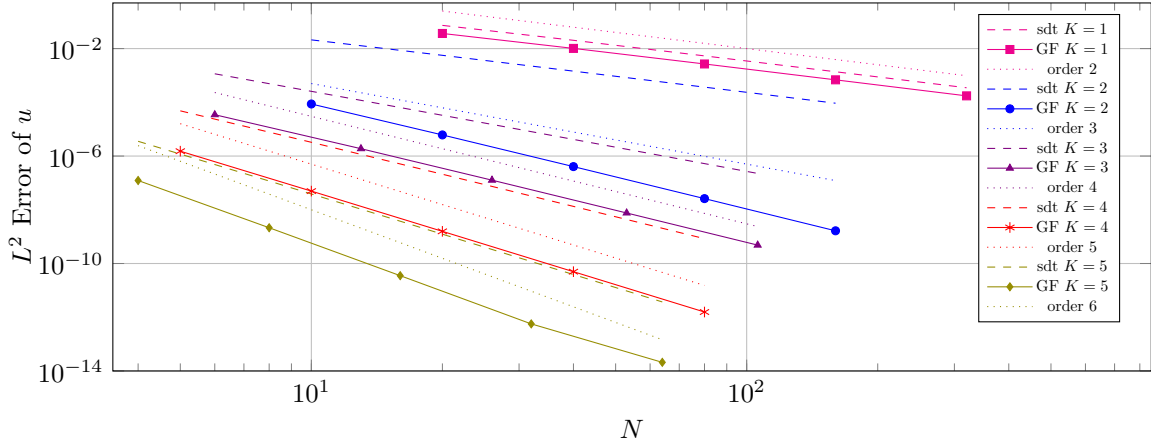


Figure 10: Stommel-Gyre: convergence of L^2 error in $\nabla \cdot \mathbf{u}$ with respect to the number of elements in x .

cluded in both computations. We find $K + 1$ accurate approximations of the divergence for polynomials of degree K , as well as reductions in the error on this operator up to several orders of magnitude for $K \geq 2$.

Finally, we run a perturbation test. To this end, for each method we run a long time simulation up to $T = 100$. We consider the state obtained to be a reasonable discrete equilibrium. Then, we add to each of these discrete states the perturbation (91), for values of ε depending on the underlying accuracy: $\varepsilon = 10^{-3}$ for Q^1 ; $\varepsilon = 10^{-5}$ for Q^2 ; $\varepsilon = 10^{-8}$ for Q^3 . We evolve these perturbations up to $T = 0.35$. In Figure 11, we see again that the perturbations, even very small ones, are well represented within few cells for the SU-GF scheme, while the standard one produces spurious waves resulting from the interaction with the source terms. As in all other cases, also for this more physical and complex test the GF schemes outperform the standard ones.

8 Conclusions and outlook

In this work, we have generalized the steady state preserving Finite Element approach based on multi-dimensional GF quadrature of [10] by including source terms of quite general forms. The relevant equilibria here are not necessarily described by a purely solenoidal constraint and a constant pressure. More general non-trivial states are determined by the balance between the derivatives of the unknowns in different directions and the source term. With GF quadrature the equations are rewritten in such a way that all these terms are treated simultaneously, and stationarity preserving stabilized Finite Element methods can be derived easily. We have characterized the discrete steady states of these methods, with a particular focus on the role of boundary conditions at steady state. We have shown applications with schemes up to order 6 to genuinely multi-dimensional benchmarks including not only Coriolis terms, as done in other works, but more general mass and momentum sources, including a physical test case well known in the meteorology community. All the results confirm the theoretical predictions: the new Finite Element schemes obtained via the multi-dimensional GF formulation are nodally super-convergent at steady state if Gauss-Lobatto points are used. Because of stationarity preservation and super-convergence, the new methods significantly outperform standard ones when considering unsteady setups close to steady states.

Future work will be dedicated to a generalization of the present continuous stabilized Finite Element approach to non-linear systems of balance laws, as well as to formulations based on discontinuous approximations. A finite-volume version of the same idea is discussed in [9] showing similar enhanced features.

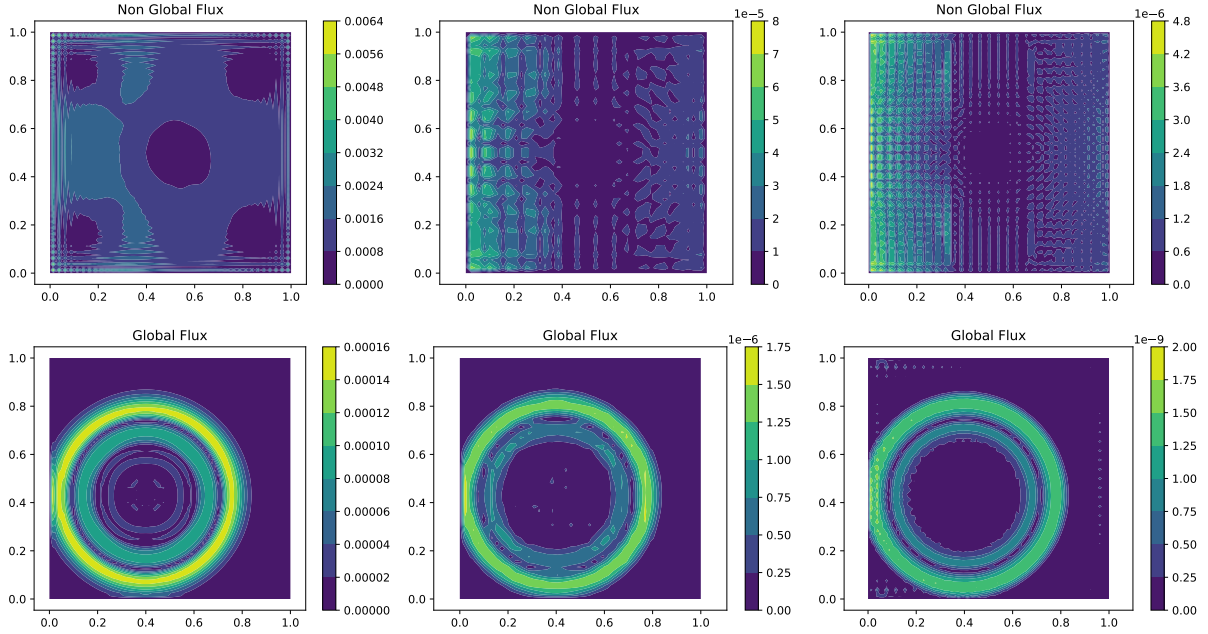


Figure 11: Perturbation test for SG: long-time equilibrium solution. Plot of $\|\mathbf{u}_{eq} - \mathbf{u}_p\|$, with \mathbf{u}_{eq} the analytical equilibrium. Left Q^1 with 80×80 cells $\varepsilon = 10^{-3}$, center Q^3 with 13 cells $\varepsilon = 10^{-5}$, right Q^3 with 26 cells $\varepsilon = 10^{-8}$

Acknowledgements

MR is a member of the team CARDAMOM, Inria research center at the University of Bordeaux.

Data availability

The data that support the findings of this study are available from the corresponding author, upon reasonable request.

Credits

All authors contributed to the study conception and design. Code development performed by Davide Torlo. The first draft of the manuscript was written by Mario Ricchiuto and all authors commented on previous versions of the manuscript. All authors read and approved the final manuscript.

A Energy stability

We study here the energy stability of the variational forms associated to the SUPG and OSS method, including Coriolis, friction, and space dependent sources, including the SU and OSS stabilizations. The results are a generalization of those already presented e.g. in [20, 19, 41, 42, 10].

A.1 Energy stability: SU stabilization

Consider a linear operator $\mathcal{L}: (C^1)^m \rightarrow (C^1)^m$,

$$\mathcal{L} = \sum_{i=1}^d \mathcal{A}_i \frac{\partial}{\partial x_i} + B, \quad A_0, \dots, A_d, B \in \mathcal{M}^{m \times m}(\mathbb{R}) \text{ constant matrices with real entries}$$

and the PDE $\partial_t \mathbf{Q} + \mathcal{L}\mathbf{Q} = 0$, $\mathbf{Q}: \mathbb{R}_0^+ \rightarrow (C^1)^m$. Consider a symmetric matrix M such that

$$E = \frac{1}{2} \int_{\Omega} \mathbf{Q}^t M \mathbf{Q} \, d\mathbf{x} =: \frac{1}{2} (\mathbf{Q}, \mathbf{Q})_M =: \frac{1}{2} \|\mathbf{Q}\|_M^2 \quad (92)$$

is the relevant energy. Define the adjoint \mathcal{L}^\dagger of \mathcal{L} as $(Q_1, \mathcal{L}Q_2)_M = (\mathcal{L}^\dagger Q_1, Q_2)_M \, \forall Q_1, Q_2$, i.e.

$$\mathcal{L}^\dagger = - \sum_{i=1}^d \mathcal{A}_i^t \frac{\partial}{\partial x_i}. \quad (93)$$

Energy preservation follows if \mathcal{L} is skew-adjoint, i.e. if $\mathcal{L} = -\mathcal{L}^\dagger$. For linear acoustics, this is the case since

$$\mathcal{L} = \begin{pmatrix} 0_{d \times d} & \text{grad} \\ \text{div} & 0 \end{pmatrix} \quad (94)$$

and $M = \mathbb{1}_{(d+1) \times (d+1)}$.

Consider now the PDE $\partial_t \mathbf{Q} + \mathcal{L}\mathbf{Q} = \mathbf{S}$ with sources $\mathbf{S}: (C^1)^m \rightarrow (C^1)^m$. Assume homogeneous or periodic boundary conditions. The SUPG method, obtained as the variational form combining (47) and (50), with \mathbf{w} a test function and $\tau \in \mathbb{R}$ reads

$$\int_{\Omega} (\mathbf{w} + \tau \mathcal{L}\mathbf{w})^t M (\partial_t \mathbf{Q} + \mathcal{L}\mathbf{Q} - \mathbf{S}) \, d\mathbf{x} = 0. \quad (95)$$

Using as test function $\mathbf{w} := \mathbf{Q} + \tau \partial_t \mathbf{Q} - \tau \mathbf{S}$ leads to

$$0 = \left(\mathbf{Q} + \tau (\partial_t \mathbf{Q} + \mathcal{L}\mathbf{Q} - \mathbf{S}) + \tau^2 \mathcal{L} \partial_t \mathbf{Q} - \tau^2 \mathcal{L}\mathbf{S}, \partial_t \mathbf{Q} + \mathcal{L}\mathbf{Q} - \mathbf{S} \right)_M \quad (96)$$

$$= (\mathbf{Q}, \partial_t \mathbf{Q})_M + \cancel{(\mathbf{Q}, \mathcal{L}\mathbf{Q})_M} - (\mathbf{Q}, \mathbf{S})_M + \tau \left(\partial_t \mathbf{Q} + \mathcal{L}\mathbf{Q} - \mathbf{S}, \partial_t \mathbf{Q} + \mathcal{L}\mathbf{Q} - \mathbf{S} \right)_M \\ + \tau^2 \left(\mathcal{L} \partial_t \mathbf{Q}, \partial_t \mathbf{Q} + \mathcal{L}\mathbf{Q} - \mathbf{S} \right)_M - \tau^2 \left(\mathbf{S}, \mathcal{L}^\dagger (\partial_t \mathbf{Q} + \mathcal{L}\mathbf{Q} - \mathbf{S}) \right)_M \quad (97)$$

$$= \frac{d}{dt} \left(E + \frac{1}{2} \tau^2 (\mathcal{L}\mathbf{Q}, \mathcal{L}\mathbf{Q})_M \right) - (\mathbf{Q}, \mathbf{S})_M + \tau \|\partial_t \mathbf{Q} + \mathcal{L}\mathbf{Q} - \mathbf{S}\|_M^2 + \tau^2 \cancel{(\mathcal{L} \partial_t \mathbf{Q}, \partial_t \mathbf{Q})_M} \quad (98)$$

$$\cancel{-\tau^2 (\mathcal{L} \partial_t \mathbf{Q}, \mathbf{S})_M} \quad \cancel{-\tau^2 (\mathbf{S}, \mathcal{L}^\dagger \partial_t \mathbf{Q})_M} - \tau^2 (\mathcal{L}\mathbf{S}, \mathcal{L}\mathbf{Q})_M + \tau^2 \cancel{(\mathbf{S}, \mathcal{L}^\dagger \mathbf{S})_M}, \quad (99)$$

where all the terms leading to integrals of the type $((\cdot), \mathcal{L}(\cdot))_M$ lead to integrals of divergences and cancel out when assuming homogeneous or periodic boundary conditions or, equivalently, because they are skew-adjoint. We are thus left with

$$\frac{d}{dt} \left(E + \frac{1}{2} \tau^2 (\mathcal{L}\mathbf{Q}, \mathcal{L}\mathbf{Q})_M \right) = (\mathbf{Q}, \mathbf{S})_M + \tau^2 (\mathcal{L}\mathbf{S}, \mathcal{L}\mathbf{Q})_M - \tau \|\partial_t \mathbf{Q} + \mathcal{L}\mathbf{Q} - \mathbf{S}\|_M^2 \leq (\mathbf{Q}, \mathbf{S})_M + \tau^2 (\mathcal{L}\mathbf{S}, \mathcal{L}\mathbf{Q})_M.$$

It is interesting to note that for the system under consideration, the SUPG energy is a triple norm associated to the following scalar product associated to the mixed space $H(\text{div}) - H^1$:

$$(\mathbf{Q}_1, \mathbf{Q}_2)_{\text{SUPG}} = \mathbf{Q}_1^t \mathbf{Q}_2 + \tau^2 (\nabla \cdot (u_1, v_1) \nabla \cdot (u_2, v_2) + \nabla p_1 \cdot \nabla p_2) \quad (100)$$

$$E_{\text{SUPG}} = \frac{1}{2} (\mathbf{Q}, \mathbf{Q})_{\text{SUPG}}. \quad (101)$$

The stability estimate can be written in terms of this scalar product as

$$\frac{d}{dt} E_{\text{SUPG}} \leq (\mathbf{Q}, \mathbf{S})_{\text{SUPG}}.$$

A.2 Energy stability: OSS stabilization

For the OSS method we can proceed in a similar abstract manner. We write the stabilized variational form as: find $\mathbf{Q} \in (V_h)^{d+1}$ such that for every $\mathbf{w} \in (V_h)^{d+1}$

$$\begin{cases} (\mathbf{w}, \partial_t \mathbf{Q} + \mathcal{L}\mathbf{Q} - \mathbf{S})_M + \tau (\mathcal{L}\mathbf{w}, \mathcal{L}\mathbf{Q} - \mathbf{S} - \Pi)_M = 0, \\ (\mathbf{w}, \Pi - (\mathcal{L}\mathbf{Q} - \mathbf{S}))_M = 0. \end{cases} \quad (102)$$

We substitute $\mathbf{w} = \mathbf{Q}$ in the first equation, and $\mathbf{w} = \Pi$ in the second and summing the two, we obtain

$$\begin{aligned} 0 &= (\mathbf{Q}, \partial_t \mathbf{Q})_M + \cancel{(\mathbf{Q}, \mathcal{L}\mathbf{Q})_M} - (\mathbf{Q}, \mathbf{S})_M + \tau (\mathcal{L}\mathbf{Q}, \mathcal{L}\mathbf{Q} - \mathbf{S} - \Pi)_M + (\Pi, \Pi - (\mathcal{L}\mathbf{Q} - \mathbf{S}))_M \\ &= (\mathbf{Q}, \partial_t \mathbf{Q})_M - (\mathbf{Q}, \mathbf{S})_M + \tau (\mathcal{L}\mathbf{Q} - \mathbf{S} - \Pi, \mathcal{L}\mathbf{Q} - \mathbf{S} - \Pi)_M + \tau \cancel{(\mathbf{S}, \mathcal{L}\mathbf{Q} - \mathbf{S} - \Pi)_M}. \end{aligned}$$

This leads to the final estimates

$$\frac{d}{dt} E = (\mathbf{Q}, \mathbf{S})_M - \tau \|\mathcal{L}\mathbf{Q} - \mathbf{S} - \Pi\|_M^2 \leq (\mathbf{Q}, \mathbf{S})_M.$$

B Proof of the consistency estimates for $S = S(x, y)$

We prove the result of proposition 7 considering the case $S = S(x, y)$ for simplicity. Let us first consider the pressure equation. By hypothesis the identity $\partial_x u_e + \partial_y v_e = S_p(x, y)$ is true in every point. It is thus true at every collocation point, and thus true for the interpolated steady operator, namely

$$\partial_x u_e(x_\alpha, y_\beta) + \partial_y v_e(x_\alpha, y_\beta) = S_p(x_\alpha, y_\beta) \quad \forall (x_\alpha, y_\beta) \implies (\partial_x u_e)_h + (\partial_y v_e)_h = (S_p)_h.$$

Crucial here is the fact that all the functions $(\partial_x u_e, \partial_y v_e$ and $S_p)$ are interpolated in the same functional space, so the interpolation of zero is consistent. Consider now the array composed by the sampled values of each term of the point-wise exact operators:

$$[Du_x^e]_{\alpha, \beta} := \partial_x u_e(x_\alpha, y_\beta), \quad [Dv_y^e]_{\alpha, \beta} := \partial_y v_e(x_\alpha, y_\beta), \quad [S_p]_{\alpha, \beta} := S_p(x_\alpha, y_\beta).$$

Trivially we have $Du_x^e + Dv_y^e - S_p^e = 0$. We thus start from the non-stabilized GF weak form and add and remove appropriate terms to errors in the projected fluxes. In particular, we remove from the discrete right hand side the array of the sampled values of the operator (which is still denoted by $(\partial_x u_e)_h + (\partial_y v_e)_h - (S_p)_h$ with some abuse of notation to allow matching terms in the proof):

$$\begin{aligned} & (D_x \otimes D_y I_y) \mathbf{u} + (D_x I_x \otimes D_y) \mathbf{v} - (D_x I_x \otimes D_y I_y) S_p \\ & \quad - (D_x \otimes D_y) (I_x \otimes I_y) \underbrace{(Du_x^e + Dv_y^e - S_p^e)}_{\equiv 0} \\ &= (D_x \otimes D_y I_y) (\mathbf{u} - (I_x \otimes \mathbb{1}_y) Du_x^e) + (D_x I_x \otimes D_y) (\mathbf{v} - (\mathbb{1}_x \otimes I_y) (\partial_y v_e)_h) \\ & \quad - \cancel{(D_x I_x \otimes D_y I_y) S_p} + \cancel{(D_x I_x \otimes D_y I_y) S_p}. \end{aligned}$$

For a fixed $y = y_\beta$, the term $\mathbf{u} - (I_x \otimes \mathbb{1}_y) (\partial_x u_e)_h$ corresponds, up to a function of y only, to the integration of

$$u'(x, y_\beta) = \partial_x u_e(x, y_\beta).$$

using the ODE solver associated to I_x . The same can be said for the term $\mathbf{v} - (\mathbb{1}_x \otimes I_y) (\partial_y v_e)_h$. We can thus construct discrete states by marching along grid-lines using the ODE solvers defined by I_x and I_y by

$$\begin{aligned} u'(x, y_\beta) &= \partial_x u_e(x, y_\beta) = -(\partial_y v_e(x, y_\beta) - S_p(x, y_\beta)), \\ v'(x_\alpha, y) &= \partial_y v_e(x_\alpha, y) = -(\partial_x u_e(x_\alpha, y) - S_p(x_\alpha, y)). \end{aligned} \quad (103)$$

By construction the resulting nodal values $u_h(x_\alpha, y_\beta)$ and $v_h(x_\alpha, y_\beta)$ verify

$$u_h + (I_x \otimes \mathbb{1}_y)((\partial_y v_e)_h - (S_p)_h) = c_x(y), \quad v_h + (\mathbb{1}_x \otimes I_y)((\partial_x u_e)_h - (S_p)_h) = c_y(x) \quad (104)$$

and are in the kernel of the above discrete operator. Moreover, they satisfy by construction the boundary estimate $(\tilde{\mathbf{v}}^\partial)_{\partial\Omega} = \tilde{\mathbf{v}}_e^\partial$ with perturbations associated to the order $\mathcal{O}(h^M)$ of the ODE integrators, while on the boundaries (x_0, y_β) and (x_α, y_0) we have exactly $(\tilde{\mathbf{v}}^\partial)_{\partial\Omega} = \mathbf{v}_e^\partial$ as initial conditions in (103). This can be shown by considering that for an arbitrary point (x_α, y_β) in the domain we have

$$\begin{aligned} u_h(x_\alpha, y_\beta) &= u_e(x_0, y_\beta) - \int_{x_0}^{x_\alpha} (\partial_y v_e(x, y_\beta) - (S_p)_h(x, y_\beta)) dx + \mathcal{O}(h^M) = u_e(x_\alpha, y_\beta) + \mathcal{O}(h^M), \\ v_h(x_\alpha, y_\beta) &= v_e(x_\alpha, y_0) - \int_{y_0}^{y_\beta} (\partial_x u_e(x_\alpha, y) - (S_p)_h(x_\alpha, y)) dy + \mathcal{O}(h^M) = v_e(x_\alpha, y_\beta) + \mathcal{O}(h^M). \end{aligned}$$

For the pressure we can immediately remark that the discrete variational form (66b) allows to define two separate discrete pressures that verify

$$\begin{aligned} \hat{p}_h(x_\alpha, y_\beta) &= p_e(x_0, y_\beta) + \int_{x_0}^{x_\alpha} (S_u)_h(x, y_\beta) dx = p_e(x_\alpha, y_\beta) + \mathcal{O}(h^M), \\ \bar{p}_h(x_\alpha, y_\beta) &= p_e(x_\alpha, y_0) + \int_{y_0}^{y_\beta} (S_v)_h(x_\alpha, y) dy = p_e(x_\alpha, y_\beta) + \mathcal{O}(h^M). \end{aligned} \quad (105)$$

By constructions these pressures satisfy the global error estimate of order $\mathcal{O}(h^M)$, and \hat{p}_h is in the kernel of the first equation of (66b) and \bar{p}_h is in the kernel of the second equation of (66b), since they verify

$$\hat{p}_h - (I_x \otimes \mathbb{1}_y)(S_u)_h = c_x(y), \quad \bar{p}_h - (\mathbb{1}_x \otimes I_y)(S_v)_h = c_y(x).$$

A unique solution of the discrete system is identified up to a compatible $\mathcal{O}(h^M)$ perturbations of the boundary data. A possibility is to set

$$p(x_\alpha, y_\beta) = \bar{p}(x_0, y_\beta) + \int_{x_0}^{x_\alpha} (S_u)_h(x, y_\beta) dx = p_e(x_0, y_0) + \int_{y_0}^{y_\beta} (S_v)_h(x_0, y) dy + \int_{x_0}^{x_\alpha} (S_u)_h(x, y_\beta) dx$$

or equivalently

$$p(x_\alpha, y_\beta) = \hat{p}(x_\alpha, y_0) + \int_{y_0}^{y_\beta} (S_v)_h(x_\alpha, y) dy = p_e(x_0, y_0) + \int_{x_0}^{x_\alpha} (S_u)_h(x, y_0) dx + \int_{y_0}^{y_\beta} (S_v)_h(x_\alpha, y) dy$$

or any linear combination $\forall \lambda \in \mathbb{R}$:

$$\begin{aligned} p(x_\alpha, y_\beta) &= p_e(x_0, y_0) + \lambda \left[\int_{y_0}^{y_\beta} (S_v)_h(x_0, y) dy + \int_{x_0}^{x_\alpha} (S_u)_h(x, y_\beta) dx \right] \\ &\quad + (1 - \lambda) \left[\int_{x_0}^{x_\alpha} (S_u)_h(x, y_0) dx + \int_{y_0}^{y_\beta} (S_v)_h(x_\alpha, y) dy \right]. \end{aligned} \quad (106)$$

To conclude, we note that the collocation method associated to the integration tables obtained from the Lagrange bases on Gauss-Lobatto points is the well known LobattoIIIA method, which verifies the hypotheses of the proposition with $M = K + 2$ when using $K + 1$ points (interpolation polynomial degree K) and $K \geq 2$ [29]. For $K = 1$ the classical h^2 consistency applies. This completes the proof.

References

- [1] R. Abgrall. High order schemes for hyperbolic problems using globally continuous approximation and avoiding mass matrices. *J.Sci.Comp.*, 73:461–494, 2017.

- [2] R. Abgrall, J. Nordström, P. Öffner, and S. Tokareva. Analysis of the SBP-SAT stabilization for finite element methods part I: linear problems. J.Sci.Comput., 85(43), 2020.
- [3] R. Abgrall and M. Ricchiuto. High order methods for CFD. In R. d. B. Erwin Stein and T. J. Hughes, editors, Encyclopedia of Computational Mechanics, Second Edition. John Wiley and Sons, 2017.
- [4] R. Abgrall and M. Ricchiuto. Hyperbolic Balance Laws: Residual Distribution, Local and Global Fluxes, pages 177–222. Springer Nature Singapore, Singapore, 2022.
- [5] E. Audusse, M. H. Do, P. Omnes, and Y. Penel. Analysis of modified Godunov type schemes for the two-dimensional linear wave equation with Coriolis source term on cartesian meshes. Journal of Computational Physics, 373:91–129, 2018.
- [6] E. Audusse, V. Dubos, N. Gaveau, and Y. Penel. Energy-stable and linearly well-balanced numerical schemes for the nonlinear shallow water equations with the coriolis force. SIAM Journal on Scientific Computing, 47(1):A1–A23, 2025.
- [7] S. Badia and R. Codina. Unified Stabilized Finite Element Formulations for the Stokes and the Darcy Problems. SIAM J.Numer.An., 47, 01 2009.
- [8] W. Barsukow. Stationarity preserving schemes for multi-dimensional linear systems. Math.Comp., 88(318):1621–1645, 2019.
- [9] W. Barsukow, M. Ciallella, M. Ricchiuto, and D. Torlo. Genuinely multi-dimensional stationarity preserving global flux finite volume formulation for nonlinear hyperbolic pdes. arXiv, 2506.21700, 2025.
- [10] W. Barsukow, M. Ricchiuto, and D. Torlo. Structure preserving nodal continuous finite elements via global flux quadrature. Numerical Methods for Partial Differential Equations, 41(1):e23167, 2025.
- [11] J. P. Berberich, P. Chandrashekar, and C. Klingenberg. High order well-balanced finite volume methods for multi-dimensional systems of hyperbolic balance laws. Computers & Fluids, 219:104858, 2021.
- [12] A. Bermudez and M. Vazquez. Upwind methods for hyperbolic conservation laws with source terms. Computers & Fluids, 23(8):1049 – 1071, 1994.
- [13] C. Birke, W. Boscheri, and C. Klingenberg. A well-balanced semi-implicit imex finite volume scheme for ideal magnetohydrodynamics at all mach numbers. J.Sci.Scomput., 98(34), 2024.
- [14] F. Bouchut, J. Le Sommer, and V. Zeitlin. Frontal geostrophic adjustment and nonlinear wave phenomena in one-dimensional rotating shallow water. Part 2. High-resolution numerical simulations. Journal of Fluid Mechanics, 514:35–63, 2004.
- [15] A. N. Brooks and T. J. Hughes. Streamline upwind/Petrov-Galerkin formulations for convection dominated flows with particular emphasis on the incompressible Navier-Stokes equations. Comput.Meth.Appl.Mech.Eng., 32(1-3):199–259, 1982.
- [16] Y. Cheng, A. Chertock, M. Herty, A. Kurganov, and T. Wu. A new approach for designing moving-water equilibria preserving schemes for the shallow water equations. J.Sci.Com., 80(1):538–554, 2019.
- [17] A. Chertock, A. Kurganov, X. Liu, Y. Liu, and T. Wu. Well-balancing via flux globalization: Applications to shallow water equations with wet/dry fronts. J.Sci.Com., 90(1):1–21, 2022.
- [18] M. Ciallella, D. Torlo, and M. Ricchiuto. Arbitrary High Order WENO Finite Volume Scheme with Flux Globalization for Moving Equilibria Preservation. J.Sci.Comp., 96:53, 2023.
- [19] R. Codina. Stabilization of incompressibility and convection through orthogonal sub-scales in finite element methods. Comput.Meth.Appl.Mech.Eng., 190(13):1579–1599, 2000.

- [20] R. Codina and J. Blasco. A finite element formulation for the Stokes problem allowing equal velocity-pressure interpolation. Comput.Meth.Appl.Mech.Eng., 143(3):373–391, 1997.
- [21] R. Comblen, J. Lambrechts, J.-F. Remacle, and V. Legat. Practical evaluation of five partly discontinuous finite element pairs for the non-conservative shallow water equations. Int.J.Numer.Meth.Fl., 63(6):701–724, 2010.
- [22] H. Deconinck and M. Ricchiuto. Residual distribution schemes: Foundations and analysis. In Encyclopedia of Computational Mechanics Second Edition, pages 1–53. John Wiley & Sons, Ltd, 2017.
- [23] M. Dumbser, O. Zanotti, E. Gaburro, and I. Peshkov. A well-balanced discontinuous galerkin method for the first-order z4 formulation of the einstein-euler system. Journal of Computational Physics, 504:112875, 2024.
- [24] A. Dutt, L. Greengard, and V. Rokhlin. Spectral deferred correction methods for ordinary differential equations. BIT, 40(2):241–266, 2000.
- [25] E. Gaburro, M. J. Castro, and M. Dumbser. Well-balanced Arbitrary-Lagrangian-Eulerian finite volume schemes on moving nonconforming meshes for the Euler equations of gas dynamics with gravity. Monthly Notices of the Royal Astronomical Society, 477(2):2251–2275, 03 2018.
- [26] L. Gascón and J. Corberán. Construction of second-order tvd schemes for nonhomogeneous hyperbolic conservation laws. J.Comput.Phys., 172(1):261–297, 2001.
- [27] L. Gascón and J. Corberán. Construction of second-order TVD schemes for nonhomogeneous hyperbolic conservation laws. J.Comput.Phys., 172(1):261–297, 2001.
- [28] E. Guerrero Fernández, C. Escalante, and M. J. Castro Díaz. Well-balanced high-order discontinuous galerkin methods for systems of balance laws. Mathematics, 10(1), 2022.
- [29] E. Hairer, G. Wanner, and S. Norset. Solving Ordinary Differential Equations I. Nonstiff problems. Springer, Berlin, Heidelberg, 1993.
- [30] T. J. Hughes and M. Mallet. A new finite element formulation for computational fluid dynamics: III. The generalized streamline operator for multidimensional advective-diffusive systems. Comput.Meth.Appl.Mech.Eng., 58(3):305–328, 1986.
- [31] R. Jeltsch and M. Torrilhon. On curl-preserving finite volume discretizations for shallow water equations. BIT Numerical Mathematics, 46(1):35–53, 2006.
- [32] J. Jung and V. Perrier. Steady low mach number flows: identification of the spurious mode and filtering method. J. Comput. Phys., 468:111462, 2022.
- [33] J. Jung and V. Perrier. Behavior of the discontinuous galerkin method for compressible flows at low mach number on triangles and tetrahedrons. SIAM J. Sci. Comput., 46(1):A452–A482, 2024.
- [34] M. Kazolea, C. Parés, and M. Ricchiuto. Approximate well-balanced WENO finite difference schemes using a global-flux quadrature method with multi-step ode integrator weights. Computers & Fluids, 296:106646, 2025.
- [35] D. A. Kopriva and G. Gassner. On the quadrature and weak form choices in collocation type discontinuous galerkin spectral element methods. Journal of Scientific Computing, 44(2):136–155, 2010.
- [36] J. LeVeque. Finite Difference Methods for Ordinary and Partial Differential Equations: Steady-State and Time-Dependent Problems. SIAM, 2007.
- [37] T. Lung and P. Roe. Toward a reduction of mesh imprinting. Int.J.Numer.Meth.Fl., 76(7):450–470, 2014.

- [38] Y. Mantri, P. Öffner, and M. Ricchiuto. Fully well-balanced entropy controlled discontinuous galerkin spectral element method for shallow water flows: Global flux quadrature and cell entropy correction. J.Comput.Phys., page 112673, 2023.
- [39] L. Micalizzi, M. Ricchiuto, and R. Abgrall. Novel well-balanced continuous interior penalty stabilizations. J.Sci.Comp., 100(14), 2023.
- [40] L. Micalizzi and D. Torlo. A new efficient explicit Deferred Correction framework: analysis and applications to hyperbolic PDEs and adaptivity. Comm.Appl.Math.Comp., 2023.
- [41] S. Michel, D. Torlo, M. Ricchiuto, and R. Abgrall. Spectral analysis of continuous FEM for hyperbolic PDEs: influence of approximation, stabilization, and time-stepping. J.Sci.Comp., 89(2):1–41, 2021.
- [42] S. Michel, D. Torlo, M. Ricchiuto, and R. Abgrall. Spectral analysis of high order continuous FEM for hyperbolic PDEs on triangular meshes: influence of approximation, stabilization, and time-stepping. J.Sci.Comp., 94:49, 2023.
- [43] M. L. Minion. Semi-implicit spectral deferred correction methods for ordinary differential equations. Comm.Math.Sci., 1(3):471–500, 2003.
- [44] S. Mishra and E. Tadmor. Constraint preserving schemes using potential-based fluxes II. genuinely multi-dimensional central schemes for systems of conservation laws. ETH preprint, (2009-32), 2009.
- [45] K. W. Morton and P. L. Roe. Vorticity-preserving Lax-Wendroff-type schemes for the system wave equation. SIAM J.Sci.Comp., 23(1):170–192, 2001.
- [46] A. T. Patera. A spectral element method for fluid dynamics: Laminar flow in a channel expansion. Journal of Computational Physics, 54(3):468–488, 1984.
- [47] M. Ricchiuto. Contributions to the development of residual discretizations for hyperbolic conservation laws with applications. Habilitation à diriger des recherches, Université Sciences et Technologies - Bordeaux I, Dec. 2011. PDF available at <https://theses.hal.science/tel-00651688/>.
- [48] M. Ricchiuto and D. Torlo. Analytical travelling vortex solutions of hyperbolic equations for validating very high order schemes. arXiv preprint arXiv:2109.10183, 2021.
- [49] P. Roe. Upwind differencing schemes for hyperbolic conservation laws with source terms. In C. Carasso, D. Serre, and P.-A. Raviart, editors, Nonlinear Hyperbolic Problems, pages 41–51, Berlin, Heidelberg, 1987. Springer Berlin Heidelberg.
- [50] D. Sidilkover. Factorizable schemes for the equations of fluid flow. Applied numerical mathematics, 41(3):423–436, 2002.
- [51] H. Stommel. The westward intensification of wind-driven ocean currents. Eos, Transactions American Geophysical Union, 29(2):202–206, 1948.